NAVAL POSTGRADUATE SCHOOL
Monterey, California

THESIS

PERTURBATIVE INVERSION OF GEOACOUSTIC PARAMETERS IN A SHALLOW WATER ENVIRONMENT

by

James Mark Null

March, 1995

Thesis Advisors: Robert H. Bourke
James H. Wilson

Approved for public release; distribution is unlimited.

DISCLAIMER NOTICE

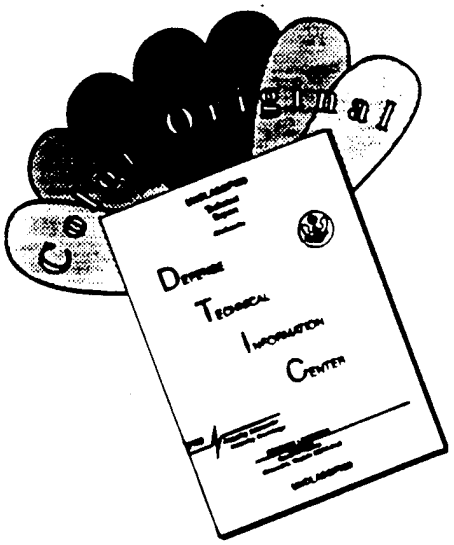

THIS DOCUMENT IS BEST QUALITY AVAILABLE. THE COPY FURNISHED TO DTIC CONTAINED A SIGNIFICANT NUMBER OF COLOR PAGES WHICH DO NOT REPRODUCE LEGIBLY ON BLACK AND WHITE MICROFICHE.

REPORT DOCUMENTATION PAGE

Form Approved OMB No. 0704-0188

1. AGENCY USE ONLY *(Leave blank)*	2. REPORT DATE	3. REPORT TYPE AND DATES COVERED
	March, 1995	Master's Thesis

4. TITLE AND SUBTITLE Perturbative Inversion of Geoacoustic Parameters in a Shallow Water Environment.	5. FUNDING NUMBERS
6. AUTHOR(S) James Mark Null	
7. PERFORMING ORGANIZATION NAME(S) AND ADDRESS(ES) Naval Postgraduate School Monterey CA 93943-5000	8. PERFORMING ORGANIZATION REPORT NUMBER
9. SPONSORING/MONITORING AGENCY NAME(S) AND ADDRESS(ES)	10. SPONSORING/MONITORING AGENCY REPORT NUMBER
11. SUPPLEMENTARY NOTES The views expressed in this thesis are those of the author and do not reflect the official policy or position of the Department of Defense or the U.S. Government.	
12a. DISTRIBUTION/AVAILABILITY STATEMENT Approved for public release; distribution is unlimited.	12b. DISTRIBUTION CODE

13. ABSTRACT *(maximum 200 words)*

In many strategic shallow water areas the geoacoustic properties of the sub-bottom are largely unknown. In this thesis it is demonstrated that inverse theory and measured data from a single hydrophone can be used to accurately deduce the geoacoustic properties of the sub-bottom, even when the initial background geoacoustic model is a highly inaccurate "guess". Since propagation in shallow water is very sensitive to the geoacoustic properties of the sub-bottom, the inverse technique developed in this thesis presents the Navy with a vitally important, practical, and inexpensive means to improve sonar performance prediction in a potentially hostile environment.

To provide ground truth for the inverse technique, measured data collected during Project GEMINI were compared to the inverse solutions. Detailed, site-specific geoacoustic models were developed for two array locations and the Finite Element Parabolic Equation (FEPE) model was used to estimate transmission loss (TL). The model estimates from FEPE compared well with the measured data and the detailed geoacoustic models were considered as "ground truth". To test the efficacy of the technique, initial background geoacoustic models were constructed assuming no *a priori* information of the bottom. The resultant inverse solution was used to predict the geoacoustic properties at each of the sites. The final results were in excellent agreement with the measured data and the resulting inverse technique TL estimates were as good or better than the TL estimates obtained from the detailed, site-specific geoacoustic models.

14. SUBJECT TERMS geoacoustic models, perturbative inversion method, Project GEMINI, FEPE, SNAP			15. NUMBER OF PAGES 98
			16. PRICE CODE
17. SECURITY CLASSIFICATION OF REPORT Unclassified	18. SECURITY CLASSIFICATION OF THIS PAGE Unclassified	19. SECURITY CLASSIFICATION OF ABSTRACT Unclassified	20. LIMITATION OF ABSTRACT UL

NSN 7540-01-280-5500 Standard Form 298 (Rev. 2-89)

Prescribed by ANSI Std. 239-18

Approved for public release; distribution is unlimited.

PERTURBATIVE INVERSION OF GEOACOUSTIC PARAMETERS IN A SHALLOW WATER ENVIRONMENT

by

James Mark Null
Lieutenant, United States Navy
B.S., The University of Texas, 1987

Submitted in partial fulfillment
of the requirements for the degrees of

MASTER OF SCIENCE IN METEOROLOGY
and
PHYSICAL OCEANOGRAPHY

from the

NAVAL POSTGRADUATE SCHOOL
March 1995

Author: James Mark Null
James Mark Null

Approved by: Robert H. Bourke
Robert H. Bourke, Thesis Advisor

James H. Wilson
James H. Wilson, Thesis Advisor

Robert H. Bourke
Robert H. Bourke, Chairman
Department of Oceanography

ABSTRACT

In many strategic shallow water areas the geoacoustic properties of the sub-bottom are largely unknown. In this thesis it is demonstrated that inverse theory and measured data from a single hydrophone can be used to accurately deduce the geoacoustic properties of the sub-bottom, even when the initial background geoacoustic model is a highly inaccurate "guess". Since propagation in shallow water is very sensitive to the geoacoustic properties of the sub-bottom, the inverse technique developed in this thesis presents the Navy with a vitally important, practical, and inexpensive means to improve sonar performance prediction in a potentially hostile environment.

To provide ground truth for the inverse technique, measured data collected during Project GEMINI were compared to the inverse solutions. Detailed, site-specific geoacoustic models were developed for two array locations and the Finite Element Parabolic Equation (FEPE) model was used to estimate transmission loss (TL). The model estimates from FEPE compared well with the measured data and the detailed geoacoustic models were considered as "ground truth". To test the efficacy of the technique, initial background geoacoustic models were constructed assuming no *a priori* information of the bottom. The resultant inverse solution was used to predict the geoacoustic properties at each of the sites. The final results were in excellent agreement with the measured data and the resulting inverse technique TL estimates were as good or better than the TL estimates obtained from the detailed, site-specific geoacoustic models.

TABLE OF CONTENTS

ACKNOWLEDGMENTS

I would like to thank and extend my highest regard for the overwhelming support, guidance, and enthusiasm of Professors James H. Wilson and Robert H. Bourke in the preparation of this thesis. I am indebted to Professor Jim Wilson for his valuable technical discussions, opinions, and active participation in all phases of this work. His inspiring confidence in geoacoustic modeling kept me going throughout the project. Professor Bob Bourke's critical review of this work provided many new and useful insights.

I am also indebted to Naval Command, Control and Ocean Surveillance Center RDT&E Division (NRaD). I am especially honored to be a recipient of the first annual NRaD fellowship program. The fellowship allowed me to plan and execute a research proposal that would not of otherwise been achieved without NRaD's generous support. Many thanks to Captain Kirk Evans, Dr. John Roese, and Dr. Homer Buccer for their overwhelming support of this program.

I am most grateful for the extraordinary support, guidance, and expertise provided by Dr. Subramaniam Rajan of Woods Hole Oceanographic Institution (WHOI). Dr. Rajan's extensive work in inversion theory sparked my enthusiasm in the subject matter. He generously provided me with numerous references and invaluable technical assistance throughout the course of this thesis. Thanks Rajan.

I am likewise indebted to Dr. Stanley Chin-Bing and Dr. David King, of NRL (Bayou Det.). Stan and Dave provided invaluable assistance in the use of FEPE. Their quick response to my many queries is truly appreciated. Paul Bucca and Bruce Gomes provided much appreciated environmental support. Additionally, I wish to thank Mrs. Josette Fabre of Neptune Sciences, Inc. for her assistance in getting the acoustic models up and running. Her diligence saved countless hours at the terminal.

Finally, I offer my sincere thanks and appreciation to my wife,

Barbara, and daughters, Jennifer, Melissa, and Courtney. They were most understanding of Daddy's strange behavior as he sequestered himself in his office. Without their support and patience, none of this would of occurred.

I. INTRODUCTION

A. NEW PRIORITIES

The United States Navy (USN) strategic vision articulated in "...From the Sea,"(O'Keefe et al., 1992) asserts U.S. naval forces as full participants in the new national strategy for the post-Cold War Era. No longer focused primarily on open ocean global conflict, the naval service's new emphasis is clearly placed on regional contingencies in the littoral regions of the world. Accordingly, the Navy has downgraded its previous anti-submarine warfare (ASW) requirements that stressed blue-water capabilities against Soviet attack and ballistic missile submarines to a more localized focus towards conventionally powered submarines operated by Third World countries.

Apart from the United States and the Commonwealth of Independent States (CIS), over 40 other countries now operate more than 400 submarines worldwide (Withers, 1992), half of which are operated by Third World countries. Some of the more modern submarine types held in Third World inventories include: the Ex-Soviet KILO-Class, the German Type 209, the British OBERON-Class and the French AGOSTA-Class. Historically, diesel electric submarine (SSK) operations have been limited in both endurance and range. However, recent developments in propulsion technology, including air independent propulsion (AIP), have substantially reduced snorkeling requirements and have also produced a quieter, more formidable SSK. Due to their smaller size, SSKs offer lower target strengths than their nuclear counterparts; they offer less of a target to ping on and thus produce less return. When operating slowly, they are non-cavitating and provide little Doppler return. The net effect of these improvements is to reduce the detection opportunities for ASW forces. In order to gain control of the seas, whether denying it to an adversary or protecting it for self use, the U. S. Navy must develop the ability to conduct successful ASW operations within the littoral environments.

B. BACKGROUND

Shallow water acoustics has long been a topic of ASW research and has been thoroughly investigated both theoretically and experimentally (e.g., Akal, 1980; Frisk et al., 1984; Rajan et al., 1987). However, the accumulation of theory and direct measurements has failed to provide consistent, accurate, and qualitative prediction of acoustic propagation in shallow water environments. The reason for this is due almost entirely to the complexity of the problem. In shallow water the acoustic medium consists of properties that vary both spatially and temporally on rather short scales. Since the spatial variation of geoacoustic properties of the bottom/sub-bottom is large, it is unlikely that a complete and accurate data base of bottom/sub-bottom geoacoustic properties will ever be collected for all shallow water areas of interest. Therefore, the U. S. Navy critically needs and accurate, cost effective, and practical method to measure or deduce the geoacoustic properties of the sub-bottom. The aim of this thesis is to solve this challenging problem vital to the U. S. Navy's ability to accurately model acoustic propagation in shallow water.

Unlike the deep-water environment, acoustic propagation in shallow water is dominated by repeated interactions with the seafloorand sub-bottom. A distinguishing characteristic of shallow water propagation is that the sound-speed profile (SSP) is generally nearly constant with depth or is downward refracting, meaning that long-range propagation takes place exclusively via bottom-interacting paths. The deep-water concept of direct path (DP) and convergence zone (CZ) acoustic propagation does not apply in the shallow water environment. Instead, the more important propagation paths are of the form of refracted bottom-reflected or surface-reflected bottom-reflected propagation. Generally, the high attenuation resulting from repeated acoustic interaction with the bottom and limited water depths severely impacts propagation, thereby reducing detection ranges in shallow

water. Figure 1 gives an example of the degree of transmission loss (TL) variability as a function of range in shallow water. The plot illustrates average TL versus range for shallow regions (100-200 m) around the world (Urick, 1979). Two features are of immediate interest in this figure. One is the spread of the TL data in excess of 50 dB at 100 km due primarily to the

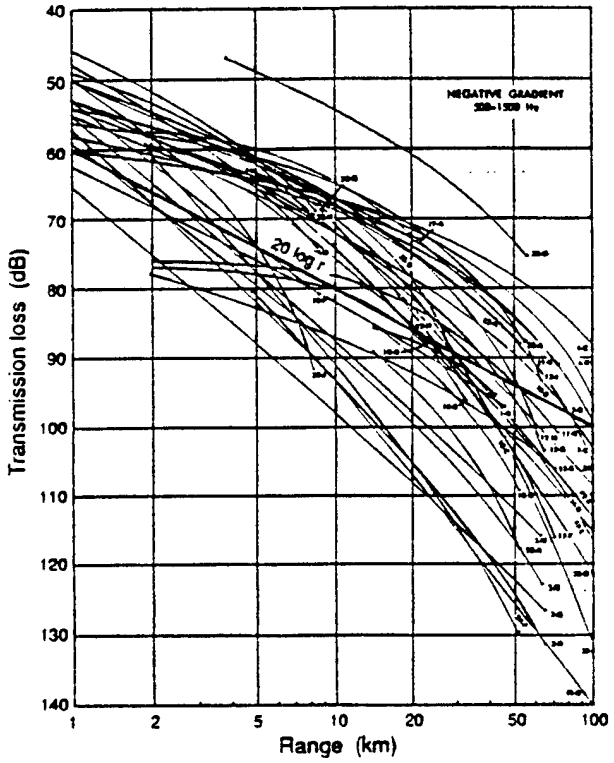

Figure 1. Transmission loss variability in shallow water (from Urick, 1979).

varying geoacoustic makeup of the seafloor. The second feature is that propagation is generally better than that experienced with spherical spreading (20 log r) at short and intermediate ranges but is larger for extended ranges. This feature is attributed to reduced spreading loss due to the trapping of acoustic energy in the shallow water wave guide which tends to decrease TL at shorter ranges. However, due to increased interaction with the boundaries, TL increases at longer ranges (Jensen et al., 1994). The

cross-over range depends on water depth, acoustic frequency, and the nature of the sea bottom.

At low frequencies acoustic propagation in shallow water is highly dependent on the geoacoustic properties of the sea bed. As sound propagates through the sea bed, the acoustic pressure field is influenced by the unique physical properties of the sedimentary sequence through which it travels and also by the nature of the lithologic boundaries. Thus, an area of considerable interest in underwater acoustics is the determination and qualitative description of these geoacoustic parameters that effect acoustic propagation. The traditional approach for describing the acoustic interaction with the bottom has been to develop a geoacoustic model (direct method) by methods described in Hamilton (1980). Provided adequate geologic and geophysical data exist in the study area, this method has proved invaluable to acoustic propagation modeling efforts.

A second approach involves the inversion of these properties from a measured sound pressure field. Numerous techniques have been cited in the literature for obtaining inverse geoacoustic solutions. Frisk et al. (1986) used amplitude versus range data obtained using a deep-towed pulsed continuous wave (CW) source and two receivers anchored near the bottom to infer geoacoustic properties of the upper sedimentary layers in deep water. The inferred geoacoustic model was derived from the measured data using an iterative forward modeling technique. The method relies on time-gating to separate the bottom reflected arrivals from the surface reflected signal. Zhou and Zhang (1987) deduced geoacoustic properties through normal mode filtering techniques. Their technique utilizes dispersion analysis and normal mode measurements to determine acoustic attenuation and propagation speeds for a horizontally stratified bottom as a function of frequency. This type of experiment requires the use of a vertical array of hydrophones to successfully separate the modal arrivals.

In this thesis we use a perturbative inversion technique (Lynch et al., 1987; Rajan, 1992) to obtain the compressional sound speed as a function of depth for the upper sedimentary layers using as input data the eigenvalues of the propagating sound field. The method consists of measuring the magnitude and phase of the pressure field as a function of range generated by a CW point source and numerically Hankel transforming these data to obtain the depth-dependent Green's function versus horizontal wavenumber. The resulting Green's function contains information about the discrete and continuous modal spectra of the waveguide; specifically the prominent peak in the Green's function occurs at wave numbers corresponding to the eigenvalues for the trapped modes of the waveguide. Although the sedimentary layers have enough rigidity to support shear wave propagation, Fryer (1978) indicates that the effect of compressional to shear wave conversion at the layer interfaces is minimal for frequencies above 20 Hz. Thus in this work, the sediments are treated as a fluid extension of the water column and the shear wave effects are neglected. Furthermore, the water column is characterized as isospeed bounded at the surface and bottom by a horizontally stratified media.

C. PROJECT GEMINI

A series of narrow-band bottom interaction experiments, collectively called Project GEMINI, were performed in the Gulf of Mexico near Corpus Christi, Texas in September 1985. Project GEMINI was designed to be a "baseline" experiment to evaluate low-frequency acoustic interaction with the seabed (Lynch et al., 1991). The intent of the experiment was to obtain high-resolution acoustic measurements at a relatively benign (i.e., geologically simple, range-independent) acoustic environment which could later be used to test or benchmark state-of-the-art acoustic propagation models. In order to properly address the performance and robustness of propagation models in shallow water, the models must first be evaluated in

regions where the physical parameters (e.g., sound speed, geologic structure, etc.) affecting acoustic propagation are well understood. A propagation model that does not perform well in a geologically simple area is less likely to perform well in more geologically complex regions. The GEMINI region is characterized by a smooth, gently sloping seafloor overlying a sequence of horizontally-layered sediments. Physical characteristics of the GEMINI seafloor such as sediment thickness, speed, and density are well-known and documented (Matthews et al., 1985). Thus, the experiment provided the opportunity to qualitatively determine how well one could predict measured acoustic data using propagation models with high quality geoacoustic information as input to the models.

Project Gemini consisted of five synthetic aperture array experiments occupying three different array locations along the continental shelf of Texas. The experiments consisted of towing a narrow-band CW source at a fixed depth with output tonals of 50 Hz and 140 Hz, away from a pair of moored receivers (Lynch et al., 1991). The track lines in each of the experiments extended from zero range at the array locations to a maximum distance of about 5000 m. The lines were oriented such that they transversed upslope from the array positions nearly perpendicular to the isobath lines. The two moored receivers were placed midway in the water column and approximately 1.5 m above the bottom, respectively. A complete listing of array locations, source and receiver combinations, and dates of the experiments are presented in Table 1.

The primary array site selected for Project GEMINI, here referred to as the Rubano Site, was previously studied by the Applied Research Laboratory, Pennsylvania State University (ARL/PSU) in 1975 (Rubano, 1980). Two alternate sites, a shallow-site to the north and a deep-site to the southeast were also incorporated into the exercise (Figure 2). The water depth for the shallow site is approximately one-half that of the Rubano site

whereas the deep-site is about twice the depth. Prior to the exercise a detailed environmental assessment of the GEMINI region was carried out by researchers at the Naval Research Laboratory-Stennis Space Center Mississippi (NRL-SSC) (Matthews et al., 1985). This environmental assessment produced an acoustical evaluation of the test site which used as input a high-resolution geoacoustic model. The geoacoustic model was constructed from the most current multi-channel seismic, bathymetric, and drill-hole information available at the time. The geoacoustic model was specifically tailored for the Rubano site although it was hoped, given the proximity of the array locations and the presumed benign geologic properties of the region, that the model could be extrapolated to the two other sites.

Experiment Number	Date	Water Depth (m)	Source Depth (m)	Receiver Depths (m)	Description
1	9/08/85	30	9	15 and 29	Rubano site
2	9/09/85	30	23	15 and 29	Rubano site
3	9/10/85	62	46	32 and 61	Deep Site
4	9/11/85	21	9	16 and 20	Shallow Site
5	9/12/85	62	9	32 and 61	Deep Site

Table 1. Description of Project GEMINI.

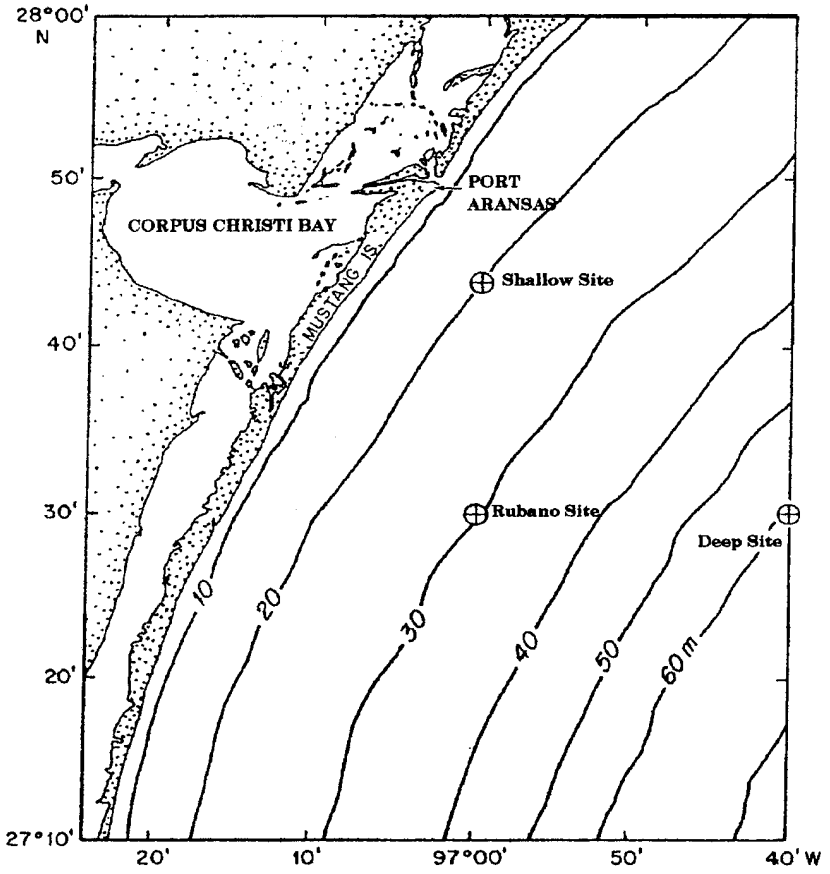

Figure 2. Geographic locations of the Project GEMINI experiments off the Texas Coast. Isobaths in meters.

D. OBJECTIVE

In shallow water the geologic and geoacoustic properties of the bottom can have significant variations over rather small ranges. Current geoacoustic modeling methods (point models) only address the physical properties of the sediment and rock as a function of depth below the sea floor at a single point and not as a function of horizontal distance. In order to adequately account for the spatial variations in geologic characteristics a

series of geoacoustic models must be developed to account for this variability. However, as stated previously, such spatially varying data are not generally available. An alternative approach is to infer these geoacoustic parameters through geoacoustic inversion techniques.

The objectives of this study are three-fold. The first objective is to compare several propagation model estimates of TL with measured low-frequency acoustic propagation data collected during Project GEMINI. Such a comparison will determine which of several TL models most closely approximates the observed TL pattern, i.e., which model solves the forward problem best. The acoustic models will have as input location-specific, high-resolution geoacoustic characterizations of the seafloor. The acoustic models that will be used in this study are the SACLANTCEN normal mode model (SNAP), the NRL normal mode model (KRAKEN), and the NRL finite element parabolic equation model (FEPE).

The second objective is to infer the geoacoustic properties of the seafloor in the GEMINI region using the perturbative inversion method. The underlying assumption of perturbative inversion theory is that a reasonable "first guess" of the unknown geoacoustic properties must be incorporated as a starting point in the computation process (Frisk et al., 1989). Using a detailed, location-specific geoacoustic model as a starting point in the inversion process, it will be shown that a geoacoustic model, derived through inversion, results in improved TL model estimates over those presented earlier.

Lastly, an objective vitally important to the Navy's operational performance in shallow water will be pursued. In many shallow water regions little geologic or geophysical information is readily available to formulate useful geoacoustic characterizations of the bottom. If, however an "educated first guess" for a geoacoustic model is made in a shallow water area of interest, it is important to determine how accurate the perturbative

inversion technique will be in estimating the actual geoacoustic properties. Moreover, the TL model results using this process must be assessed to see how comparable they are to those formulated using a high quality geoacoustic model as an input.

II. NORMAL MODE SOLUTIONS IN A WAVEGUIDE

A. MODAL PROPAGATION

The inverse method considered in this thesis requires as input data the measured horizontal wave numbers or eigenvalues which characterize the modal propagation of sound through the ocean and seafloor. Since the ideas presented in normal mode theory are essential to the inversion process, a brief discussion of normal mode propagation is presented. Normal mode theory provides a 'full wave' solution of the wave equation in the ocean waveguide which takes into account the physical characteristics of the medium, frequency dispersion effects, and interaction of the sound field at the boundaries (Casey, 1988).

The propagation of monochromatic sound in the ocean is described mathematically by solutions to the reduced wave or Helmholtz equation. Using the assumption of cylindrical symmetry, the spatial part of the acoustic pressure $p(r,z,z_o)$, due to a point source at range $r = 0$ and depth $z = z_o$ with a sinusoidal or harmonic time dependence $\exp(-i\omega t)$, satisfies the Helmholtz equation

$$\left[\frac{1}{r}\frac{\partial}{\partial r}\left(r\frac{\partial}{\partial r}\right)+\frac{\partial^2}{\partial z^2}+k^2(z)\right]p(r,z,z_o)=\frac{-2\delta(z-z_o)}{r}\delta(r) \qquad (1)$$

where $p(r,z,z_o)$ represents the acoustic pressure at range r and depth z, ω is the radian frequency, and $k(z) = \omega/c(z)$ is the total wave number.

Appropriate boundary conditions must be specified in order to determine a unique solution to Equation (1). At the interfaces where there are significant variations in properties, e.g., at the water sediment interface, continuity of pressure and normal particle velocity must be met. The symmetry and range independence of Equation (1) leads to the method of

separation of variables in solving the equation. By expressing the pressure field $p(r;z,z_o)$ by

$$p(r,z,z_o) = Z(z)R(r) \tag{2}$$

and substituting this into Equation (1) leads to the following expression

$$\frac{1}{R}\left[\frac{1}{r}\frac{d}{dr}\left(r\frac{dR}{dr}\right)\right]+\frac{1}{Z}\left[\rho(z)\frac{d^2Z}{dz^2}\right]+k^2=0 \tag{3}$$

The first term in Equation (3) is a function of r only whereas the second term is a function of z only. This equality is satisfied if and only if both expressions are equal to the same constant of proportionality which leads to the two separated equations:

$$\frac{d^2R(r)}{dr^2}+\frac{1}{r}\frac{dR(r)}{dr}+k_r^2R(r)=0 \tag{4}$$

and

$$\frac{d^2Z(z)}{dz^2}+k_z^2Z(z)=0 \tag{5}$$

where $(k_r)^2$ and $(k_z)^2$ are the separation constants defined by

$$k_z^2 = k^2(z) - k_r^2 \tag{6}$$

Equation (4) is a function of range only, and thus from Equation (6) k_r, the horizontal component of the wave number, must be constant throughout the waveguide. This can also be expressed in terms of Snell's law since

$$k_r = k\sin\theta = \frac{\omega}{c}\sin\theta \tag{7}$$

where θ is the vertical angle of incidence and ω is constant, and $(\sin\theta)/c$ is constant (Clay and Medwin, 1977). Accordingly, at a zero incidence angle ($\theta = 0°$), there is no horizontal contribution to the total wavenumber. The solution to Equation (4) is a cylindrical Bessel or Hankel function of the zeroth order.

$$R(r) = H_o^{(1)}(k_r r) \tag{8}$$

For distances of more than a few wavelengths from the source, the asymptotic expansion of $H_o^{(1)}(k_r r)$ (Haberman, 1987) can be expressed as

$$H_o^{(1)}(k_r r) \approx \sqrt{\frac{2}{\pi k_r r}} \cos\left(k_r - \frac{\pi}{4}\right) \tag{9}$$

The exponential expansion of the cosine term in Equation (9) yields the following characteristic equation

$$H_o^{(1)}(k_r r) \approx \sqrt{\frac{2}{\pi k_r r}}\left[\exp\left(ik_r r - \frac{i\pi}{4}\right) + \exp\left(-ik_r r + \frac{i\pi}{4}\right)\right] \tag{10}$$

When associated with a harmonic time dependent term, Equation (10) represents the total wave motion consisting of an inward propagating wave represented by the first term on the right side of Equation (10) and an outward propagating wave represented by the second term on the right of Equation (10). Since we are only interested in an outward propagating, exponentially decaying waveform, only the second term is used in the formulation (Clay and Medwin, 1977).

$$H_o^{(1)}(k_r r) \approx \sqrt{\frac{2}{\pi k_r}} \exp\left[-i\left(k_r r - \frac{\pi}{4}\right)\right] \tag{11}$$

1. Rigid Bottom Solution

Assuming that the ocean surface represents a pressure release surface and that the ocean bottom at z = h is perfectly rigid, allowing no acoustic penetration, the "normal mode" differential equation (Equation (5)) and the accompanying boundary conditions are:

$$\frac{d^2Z(z)}{dz^2} + k_z^2 Z(z) = 0 \tag{12}$$

$$Z(0)=0\,, \qquad \frac{dZ(h)}{dz} = 0 \tag{13}$$

By solving this equation as a Sturm-Liouville eigenvalue problem, the general solution to Equation (12) is of the form

$$Z(z)=C_1\sin(k_z z)+C_2\cos(k_z z) \tag{14}$$

where C_1 and C_2 are arbitrary constants and k_z is the vertical wavenumber. The boundary condition at the free surface (z=0) requires that the acoustic

pressure to be zero for all range, r, and time, t, thus requiring $C_2=0$. Furthermore, an incident plane wave on the sea surface is assumed to be completely reflected, undergoing a 180° phase shift upon interaction with the free surface. The rigid bottom boundary condition is characterized by the constraint that the acoustic pressure is a maxima at the seafloor at z=h and that the normal particle velocity vanishes on the surface resulting in complete reflection (Casey, 1988). This means that $k_z z = \pi/2, 3\pi/2, 5\pi/2...$ or more generally

$$(k_z)_m = (\pi/h)(2m-1), \quad m = 1, 2, 3 ... \tag{15}$$

$(k_z)_m$ is termed an eigenvalue and the solution is an eigenfunction (normal mode) of the problem. There exists an infinite number of eigenvalues and thereby an infinite number of eigenfunctions $Z_m(z)$ as solutions to this boundary value problem. Each solution is characterized by a mode shape $Z_m(z)$ and a vertical propagation constant $(k_z)_m$. The subscript m designates the modal number for a particular eigenvalue or eigenfunction.

The pressure field in Equation (2) can now be written as

$$p(r,z) = \sum_{m=1}^{\infty} R_m(r) Z_m(z) \tag{16}$$

Substituting this expression for pressure into Equation (1) yields:

$$\sum_{m=1}^{\infty}\left[\frac{1}{r}\frac{d}{dr}\left(r\frac{dR_m}{dr}\right)Z_m + k_z^2 R_m Z_m\right] = \frac{-\delta(r)\delta(z-z_o)}{2\pi r} \tag{17}$$

The eigenfunctions of the Sturm-Liouville problem form an orthonormal set of square integrable functions on 0<h<z such that

$$\int_0^h \frac{Z_m(z)Z_n(z)}{\rho(z)}dz = \begin{cases} 0 & m \neq n \\ 1 & m = n \end{cases} \tag{18}$$

Multiplying both sides of Equation (17) by

$$\int_0^h \frac{Z_n(z)}{\rho(z)}dz \tag{19}$$

and applying the orthogonality relationship of (18) yields the following

$$\frac{1}{r}\frac{d}{dr}\left(r\frac{dR_m}{dr}\right)+k_{r_m}^2 R_m=\frac{-\delta(r)Z_m(z_o)}{2\pi r\rho(z_o)} \qquad (20)$$

The solution to Equation (20) is a Hankel function of the first kind such that

$$R_m(r)=\frac{i}{4\rho(z_o)}Z_m(z_o)H_o^{(1)}(k_{r_m}r) \qquad (21)$$

Substituting the expression for $H_o^{(1)}(k_r r)(k_n r)$ found in Equation (11), the solution to Equation (1) can be expressed as a sum of normal modes

$$p(r,z,z_o)=\frac{i}{\rho(z_o)\sqrt{8\pi r}}\exp(\tfrac{-i\pi}{4})\sum_m^{\infty} Z_m(z)Z_m(z_o)\frac{\exp(ik_{r_m}r)}{\sqrt{k_{r_m}}} \qquad (22)$$

Equation (22) describes the pressure field as a linear superposition of traveling cylindrical waves propagating outward from a source. Each of these modes is a standing wave in the vertical direction with a unique depth distribution described by the eigenfunction $Z_m(z)$ and the vertical modal wavenumber $(k_z)_m$. The vertical wavenumber must ensure that a pressure node exists at the surface and, in the case of a perfectly rigid bottom, a pressure anti-node at the seafloor. The eigenfunctions $Z_m(z)$ essentially determine the depth dependence of the acoustic pressure field. For a given water depth and source frequency, only a finite number of modes may exist. For large mode numbers m, the horizontal wavenumber becomes imaginary and the solution defined by Equation (22) rapidly decays with increased horizontal ranges.

2. Penetrable Bottom Solution

If the ocean bottom is not a perfect reflector, sound energy will penetrate into the sea bed and solutions to the Helmholtz equation must be found both in the water column and the ocean bottom. The solution to Equation (1) for the penetrable bottom case can be obtained by utilizing the Green's function technique. The conditions imposed upon this case are the same as that of the rigid bottom with the exception that the velocity

potential is discontinuous at the seafloor. A brief derivation of the Green's function is now given.

Assuming a constant density water column of thickness (h), sound speed c(z), bounded at the surface and bottom by a horizontally stratified medium (Figure 3), the spatial part of the sound pressure field (p) due to a harmonic time dependent point source located at r = 0 and z = z_o satisfies Equation (1).

The solution to Equation (1) can now be written as the zero-order Hankel transform of the depth-dependent Green's function $g(k_r,z)$. This is achieved by taking the zero-order Hankel transform of both sides of Equation (1) where the Hankel transform pair is defined by the following:

$$p(r,z,) = \int_0^\infty g(k_r,z)J_o(k_r r)k_r dk_r \qquad (23)$$

$$g(k_r,z) = \int_0^\infty p(r)J_o(k_r r)rdr \qquad (24)$$

The Hankel transform variable, k_r, transforms the solution from a depth and range space p(z,r) to a solution as a function of depth and horizontal wave number space (z, k_r) (Evans, 1975).

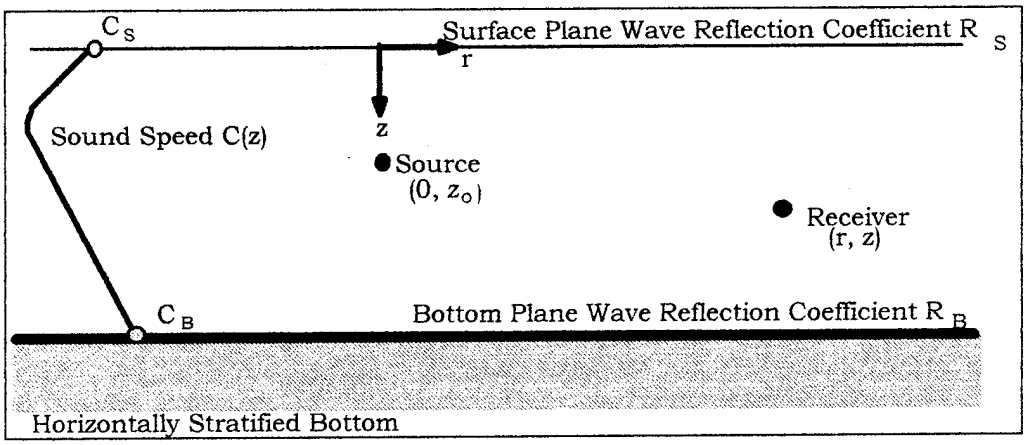

Figure 3. Horizontally stratified ocean model.

After applying Equation (24) to Equation (1) and re-ordering terms, Equation (1) is transformed into the depth separated wave equation

$$\left[\frac{d^2}{dz^2}+k^2(z)-k_r\right]g(k_r,z,z_o)=-2\delta(z-z_o) \qquad (25)$$

Here $g(k_r,z)$ is the depth-dependent Green's function, J_o is the zero-order Bessel function, r is horizontal range, and k_r is the horizontal wave number. The general solution to Equation (25) can be written as the sum of the particular solution (non-homogeneous part) and the characteristic solution (homogenous part). The characteristic solution of Equation (25) is of the form

$$g(k_r) = \phi_S+\phi_B \qquad (26)$$

where ϕ_S and ϕ_B are linearly independent solutions of Equation (25) chosen such that ϕ_S satisfies the surface boundary condition, and ϕ_B satisfies the bottom boundary condition. By applying the method of variation of parameters, the Green's function can be defined by:

$$g(k_r,z) = \frac{-2\phi_S(k_r,z)\phi_B(k_r,z_o)}{W(z_o)} \qquad 0 \le z \le z_o \qquad (27)$$

$$g(k_r,z) = \frac{-2\phi_S(k_r,z_o)\phi_B(k_r,z)}{W(z_o)} \qquad z_o \le z \le h \qquad (28)$$

such that $W(z_o)$ is the Wronskian given by

$$W(z_o) = \phi_B(z_o)\,\phi'_S(z_o) - \phi'_B(z_o)\,\phi_S(z_o) \qquad (29)$$

where the prime indicates differentiation with respect to z. ϕ_S and ϕ_B also must satisfy the following impedance relations.

$$\frac{\phi_B}{\partial\phi_B/\partial z} = \xi_B \text{ at } z = 0$$
$$\frac{\phi_S}{\partial\phi_S/\partial z} = \xi_S \text{ at } z = h \qquad (30)$$

ξ_B and ξ_s are input quantities that contain boundary conditions necessary for the calculation of the Green's function (Frisk et al., 1980). Both quantities are dependent on the horizontal wavenumber, frequency, and the acoustic

properties of the bottom and the surface. ξ_B depends on the water density, ρ_w, and the sound speed c(z), at the water-bottom interface, while ξ_S depends on ρ_w and the sound speed c(z) at the water-surface interface. Equation (30) therefore can be expressed in terms of plane wave reflection coefficients, R_B and R_S, for the half-space corresponding to sound speed c_B and c_S bounding the bottom and the surface, respectively.

$$\phi_B(z) = C_1[\exp(-ik_z z) + R_B(k_r)\exp(ik_z z)] \tag{31}$$

$$\phi_S(z) = C_2[\exp(-ik_z z) + R_s(k_r)\exp(ik_z z)] \tag{32}$$

where $k_z^2+k_r^2 = k^2=(\omega/c)^2$ is the total wavenumber and C_1, C_2 being arbitrary constants. Equation (31) can also be re-written as

$$\xi_B = \frac{\phi_B}{\phi_B'} = \frac{i(1+R_B)}{k_z(1-R_B)}, \text{ at } z = 0 \tag{33}$$

$$\xi_S = \frac{\phi_S}{\phi_S'} = \frac{-i}{k_z}\left[\frac{1+R_S\exp(-2ik_Z h)}{1-R_S\exp(-2ik_Z h)}\right], \text{ at } z = h \tag{34}$$

Substituting these expressions into Equations (27) and (28) and further assuming that the ocean surface is a pressure release boundary (i.e., $R_S = -1$), the following expression for the depth dependent Green's function can be found:

$$g(k_r,z) = \frac{e^{ik_z z-} - e^{ik_z z+} + R_B(k_r)e^{2ik_z h}\left[e^{-ik_z z+} - e^{-ik_z z-}\right]}{-ik_z\left[1+R_B(k_r)e^{2ik_z h}\right]} \tag{35}$$

where $z+ = z+z_o$, $z- = |z-z_o|$.

In order to evaluate the integral expression for p(r,z) the Bessel function, $J_o(k_r r)$ in Equation (23), is expressed in terms of Hankel functions as:

$$J_o(k_r r) = \frac{1}{2}\left[H_0^{(1)}(k_r r) + H_0^{(2)}(k_r r)\right] \qquad (36)$$

The following relation

$$\left[H_0^{(2)} \exp(-i\pi k_r r) = -H_0^{(1)}(k_r r)\right] \qquad (37)$$

allows the range of integration of the transform integral to be evaluated over the entire real k_r axis from $-\infty$ to ∞ (Casey, 1988). The solution of Equation (23) is then found through contour integration methods (Evans, 1975) and is expressed as the sum of discrete and continuous portions of the normal mode spectrum given by

$$p(r,z) = i\pi \sum_{1}^{m} Z_m(z) Z_m(z_o) H_0^{(1)}(k_{r_m} r) + I(r) \qquad (38)$$

where the eigenvalues k_m and eigenfunctions Z_m satisfy

$$\left(\frac{d^2}{dz^2} + k^2(z) - k_{r_m}^2\right) Z_m(z) = 0 \qquad (39)$$

The discrete sum in Equation (38) corresponds to modes perfectly trapped in the waveguide and is of the same form as that of the rigid bottom solution. Typically, this trapped mode sum dominates the long range behavior of the acoustic field whereas the continuum contribution I(r) is only significant at short ranges (Lynch et al., 1987). The continuum is rapidly attenuated with increasing range from the source and is typically neglected for ranges over a few wavelengths from the source. The eigenvalues for the penetrable bottom case have the same interpretation as those in the rigid bottom solution. However, they will take on different values since sound is propagating in both the water column and the sub-bottom and the characteristic equation will be different.

The modal representation is closely correlated with the analytic properties of the Green's function. A knowledge of the behavior of $g(k_r)$ (for example, the number of resonances and their spatial location in regard to horizontal wavenumber) provides information about the nature of the modal

propagation in the waveguide. The Green's function is characterized by a finite valued continuum with a discrete set of resonances occurring when the denominator of Equation (34) is set equal to zero. These poles of $g(k_r,z)$ correspond to the eigenvalues of the trapped and virtual modes excited in the waveguide. The position and magnitudes are highly influenced by the inherent acoustic properties of the bottom (Frisk et al., 1986) and the geometry of the waveguide. As a result, the basic principle underlying the inverse method presented in this paper is first to obtain an estimate of $g(k_r)$ from measurements of p(r) by numerically performing the Hankel transform in Equation (23). The modal features of $g(k_r)$ are then used to determine a geoacoustic model. A specific perturbation technique relating the eigenvalues of the trapped modes to the geoacoustic model are given in the next section.

B. PERTURBATIVE INVERSION TECHNIQUE

A detailed discussion of the perturbative inversion theory that is the basis for the analysis in this thesis is presented in Rajan et al. (1987). The objective of the perturbative inversion technique is to estimate the variation in geoacoustic parameters (i.e., sound speed, density, attenuation, etc.) from the differences between the measured eigenvalues and the eigenvalues computed for a background geoacoustic model (Frisk et al., 1986). In the perturbative technique, an initial background geoacoustic model is assumed and the differences of the geoacoustic parameters from the geoacoustic parameters in the initial background model are calculated. For the purpose of this thesis, we are concerned with determining only the compressional sound speed profile in the bottom, *c(z)*, for the deep and shallow GEMINI sites. Perturbative techniques to determine other geoacoustic parameters (i.e., density, attenuation, etc.) are not addressed. However, these parameters can be modified to be geologically consistent with the final estimate of *c(z)*. As a first step, an initial background geoacoustic model for

$c(z)$ is assumed, and a major objective of this thesis is to evaluate the perturbative technique when the initial estimate of $c(z)$ must be based on little to no geoacoustic information about the area. Perturbation theory then provides the means for determining the difference $\Delta c(z)$ between the background model and the true earth model.

From first-order perturbation theory, an integral equation relating the perturbation of eigenvalues is given by:

$$\Delta k_m = \int_0^\infty \frac{|Z_m|^2 k(z)^2}{k_m \rho_o c_o(z)} \Delta c(z) dz \qquad (40)$$

where Δk_m represents the difference between the experimentally measured modal eigenvalues and the eigenvalues computed from the background geoacoustic model, k_m and $Z_m(z)$ are the mth eigenvalues and normalized eigenfunctions for some assumed background geoacoustic model, $\rho(z)$ is the density profile for the background geoacoustic model, $k(z)$ is the acoustic wavenumber defined by $\omega/c(z)$ (where ω is the angular frequency and $c(z)$ is sound speed profile of the geoacoustic model), and $\Delta c(z)$ is the difference in sound speed between the background and true models. All terms in Equation (40) are known except for $\Delta c(z)$ which is the solution being sought.

Equation (40) is a Fredholm integral equation of the first kind for $\Delta c(z)$ and generally does not produce a unique solution unless constraints are made upon its solution (Lynch et al., 1987). Reordering the known quantities in Equation (40) such that

$$K(m,z) = \frac{|Z_m|^2 k(z)^2}{k_m \rho_o c_o(z)} \qquad (41)$$

results in

$$\Delta k_m = \int_0^\infty K(m,z)\, \Delta c(z) dz \qquad (42)$$

$K(m,z)$ is defined as the kernel of the integral equation and consists of the known physical parameters for a discrete mode and depth step. Using methods proposed by Backus and Gilbert (1970), a solution for $\Delta c(z)$ is given by:

$$\Delta c(z) = \sum_m \sum_n K(m,z) \Delta k_m A^{-1}(m,n) \tag{43}$$

where $A(m,n)$ is the spectral decomposition of the kernel $K(m,z)$ and

$$A(m,n) = \int_a^b K(m,z) K^T(n,z) dz \tag{44}$$

The solution given by Equation (43) is called the Backus-Gilbert solution for perfect data. This solution represents the most "Dirac delta like" resolution kernel and was used in this analysis because smoothing the solution was not desirable until after $c(z)$ was estimated. This represents a solution without constraints and is considered a fundamental property of the perturbative technique not addressed originally in Rajan et al., (1987). If constraints are used in the solution for $c(z)$, the most natural (i.e., unconstrained) solution characteristics will not be realized. The "price to pay" for the natural or "unconstrained" approach is instability in the solution when the ratio of the highest to lowest eigenvalue is large. In that instance, it is well known that the pseudo-inverse to the matrix in Equation (44) is ill conditioned, but a stabilization technique based on the Frobenious norm was used. Also, a simple "box car" average of c(z) in depth was performed to dampen fluctuations in $c(z)$ with depth.

As a first step to the inversion process, measured complex pressure field versus range data was transformed from the range domain to the horizontal wave number domain (depth-dependent Green's function) via the Hankel transform pair. As discussed earlier, the normal modes of the waveguide show up as strong resonance peaks. The measured modal eigenvalues are experimentally measured by simply picking the peaklocations in $|g(k_r)|$ (Lynch et al., 1991). Figure 4 is a typical Green's

function versus horizontal wavenumber plot for a particular environment. In this instance, each of the peaks (modes 1-4) has a characteristic wavenumber or eigenvalue identified in our formulation as k_{meas}.

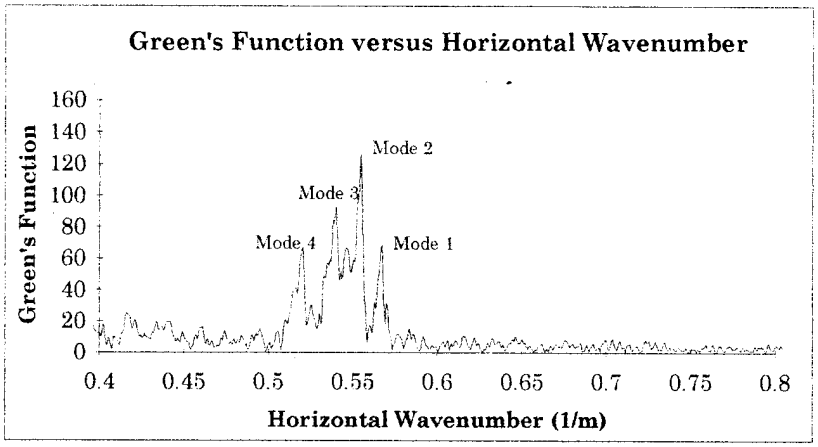

Figure 4. Plot of the depth-dependent Green's function |g(kr)| versus horizontal wavenumber k at 140 Hz. The normal modes of the particular waveguide are identified by poles of g(kr).

The NRL normal mode model, KRAKEN, was used to calculate the modal eigenvalues and eigenfunctions, k_m and $Z_m(z)$, respectively, using the assumed background geoacoustic model. In this section we assume a background geoacoustic model with a linear sound speed gradient and with constant density and attenuation with depth to illustrate the basic concepts of the inversion technique. In order to demonstrate the effectiveness of the perturbative inversion technique, the initial sound speed at the water-bottom interface and the sound speed gradient were also varied. Once k_m and $Z_m(z)$ are calculated, Δk_m is found by the relation

$$\Delta k_m = k_{meas} - k_m \qquad (m=1,2,3...) \qquad (45)$$

These values were entered into Equation (41) and the result, $\Delta c(z)$, is calculated by Equation (43) and represents the perturbation of the sound speed profile about that proposed in the initial background model. The sound

speed profile is then adjusted by subtracting $\Delta c(z)$ from the initial value of $c(z)$. The perturbative process continues until $\Delta c(z)$ is minimized.

1. Synthetic Test Cases

In this section we will apply the perturbative inversion technique to a set of synthetic data for which the correct solution is known. The synthetic earth model along with the two initial background geoacoustic models are shown in Figure 5. The synthetic earth model consists of a 50 m thick isospeed water column (1500 m/s), overlying a 10 m thick isospeed sediment layer (1800 m/s), which comformably lies over a 60 m thick linear gradient (∇c =1.50 s^{-1}) sedimentary layer. The basement consists of an isospeed half-space with a compressional wave speed of 1900 m/s. The density is assumed to be constant ρ = 1.6 g/cm^3 for all sediment layers and half-spaces. Although the water column sound speed profile for this example is assumed to be isospeed, it can consist of any structure. In general, the water column profile will be known from available XBT and CTD measurements and will thus drop out of the perturbation integrals, leaving only the sediment properties to be determined (Rajan et al., 1987).

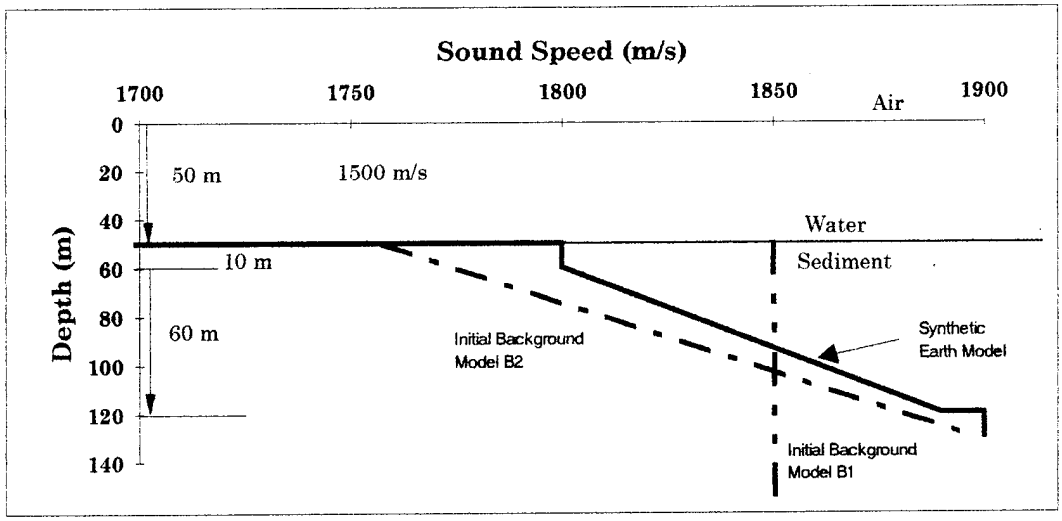

Figure 5. Properties of the synthetic earth and two backgound model.

The frequencies that will be considered in the synthetic examples are 25, 50 and 150 Hz. Sub-bottom penetration by acoustic energy is highly dependent on frequency with lower frequencies being able to penetrate deeper into the seafloor than higher frequencies. As a result, lower frequencies are able to resolve the deeper sedimentary structure, whereas the higher frequencies resolve the finer near-surface structure. The synthetic Green's function versus horizontal wavenumber plots for each of the frequencies are shown in Figures 6a-c These poles of $g(k_r,z)$, as discussed previously, correspond to the eigenvalues of the trapped and virtual modes that are excited for the particular waveguide at the given frequency. In general, higher frequencies excite more modes and thus have more trapped eigenvalues than do lower frequencies. The modal eigenvalues for the synthetic earth model (k_{meas}) are listed in Table 2.

Two initial geoacoustic background models were assumed in this example: (1) an 1850 m/s isospeed model, and (2) a linear gradient model c(z) = 1750 + 2.0 s^{-1}(z). For the purposes of these test cases, density was taken to be a constant ρ = 1.6 g/cm^3, and compressional attenuation was assumed negligible. The modeled eigenvalues (k_m) for the initial background models are shown in Tables 3 and 4.

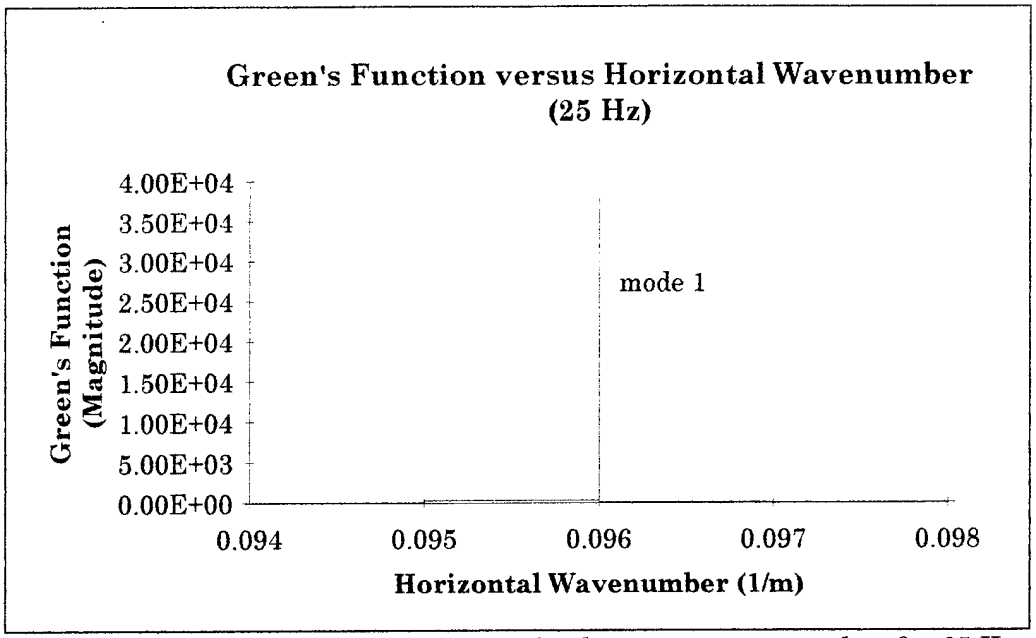

Figure 6. Synthetic Green's function magnitude versus wavenumber for 25 Hz.

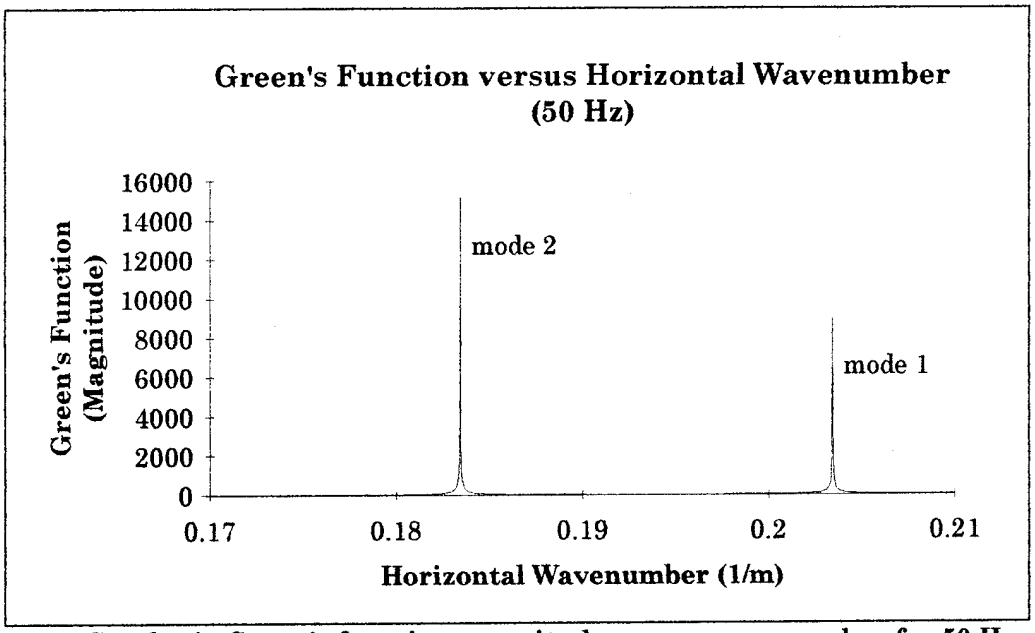

Figure 7. Synthetic Green's function magnitude versus wavenumber for 50 Hz.

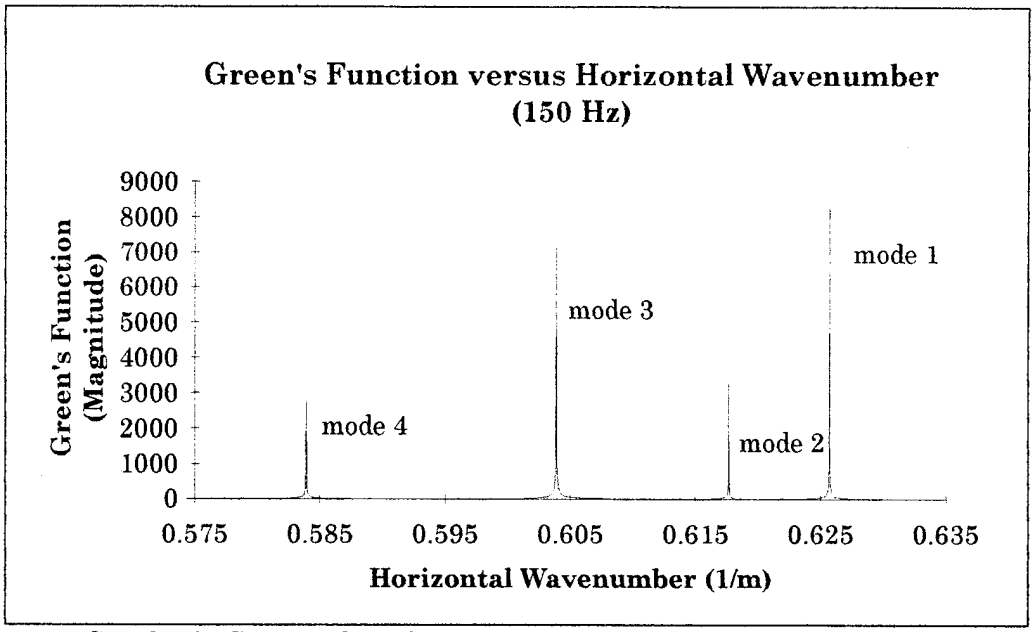

Figure 8. Synthetic Green's function magnitude versus wavenumber for 150 Hz.

Model	Frequency (Hz)	Mode	Eigenvalue (k_{meas}) (m^{-1})
Synthetic Earth Model	25	1	0.095839053
	50	1	0.203429401
	50	2	0.183431700
	150	1	0.625674903
	150	2	0.603864372
	150	3	0.617630422
	150	4	0.583889604

Table 2. Modal eigenvalues for the synthetic earth model (k_{meas}).

Model	Frequency (Hz)	Eigenvalue Iteration 1	Eigenvalue Iteration 2	Eigenvalue Iteration 3	Eigenvalue Iteration 4
Background	25	0.095567562	0.095840216		
Model B2					
	50	0.203297004	0.203447193	0.203428298	
	50	0.182848796	0.183509603	0.183428794	
	150	0.625649512	0.625688612	0.625676215	0.625808477
	150	0.617533207	0.617683887	0.617635310	0.618125618
	150	0.603655517	0.603984475	0.603875697	0.604930580
	150	0.583521008	0.584122181	0.583913684	0.587231219

Table 3. Modal eigenvalues for the initial background geoacoustic model B1 (k_m).

Model	Frequency (Hz)	Eigenvalue Iteration 1	Eigenvalue Iteration 2	Eigenvalue Iteration 3	Eigenvalue Iteration 4
Background	25	0.096081510	0.095852643	0.095839143	
Model B2					
	50	0.203560099	0.203439906	0.203429595	
	50	0.183980197	0.183473706	0.183432102	
	150	0.625703216	0.625677884	0.625686586	
	150	0.617737293	0.617641628	0.617674530	
	150	0.604090273	0.603888690	0.603957891	
	150	0.584284186	0.583935380	0.584054530	

Table 4. Modal eigenvalues for the initial background geoacoustic model B2 (k_m).

Tables 3 and 4 list the computed eigenvalues for the initial background models for each iteration in the inversion process. These eigenvalues (k_m), as discussed previously, are subtracted from the measured eigenvalues (Table 2) to form the data vector $\Delta k(m)$. Generally, the lower frequencies (i.e., fewer modes) required fewer iterations in order for solutions to converge. Figures 9-11 display the results of the pertubative inversion technique to recover the synthetic earth sound speed profile from the initial background model B1.

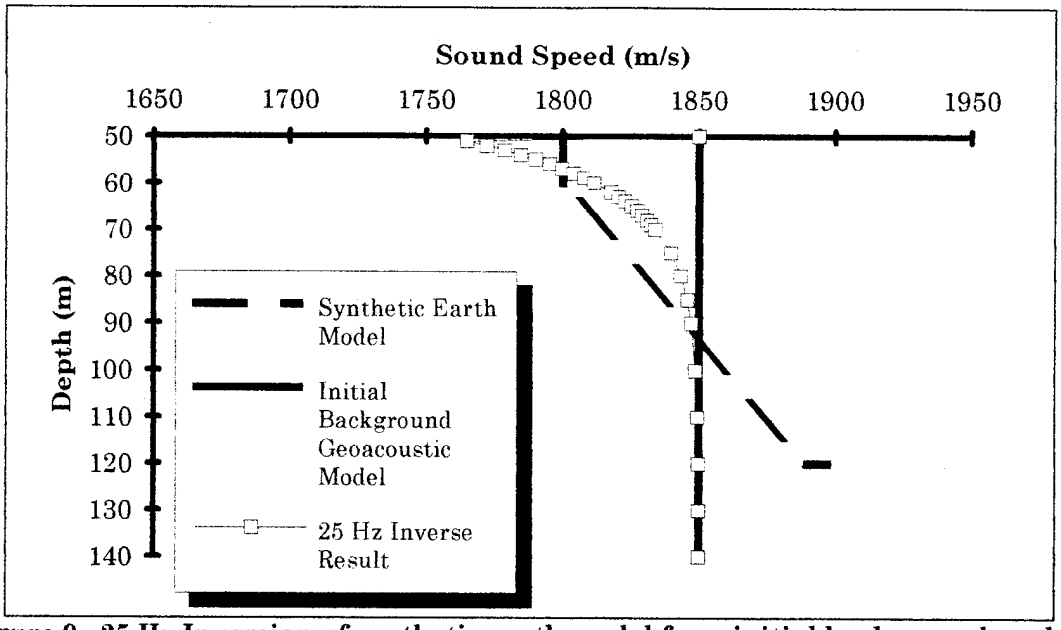

Figure 9. 25 Hz Inversion of synthetic earth model from initial background model B1.

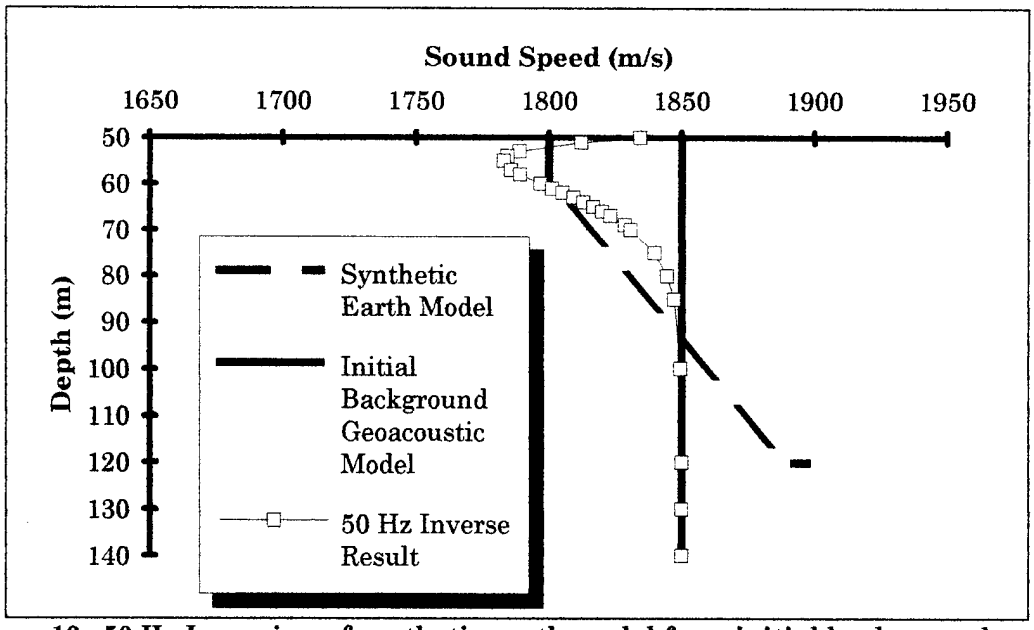

Figure 10. 50 Hz Inversion of synthetic earth model from initial background model B1.

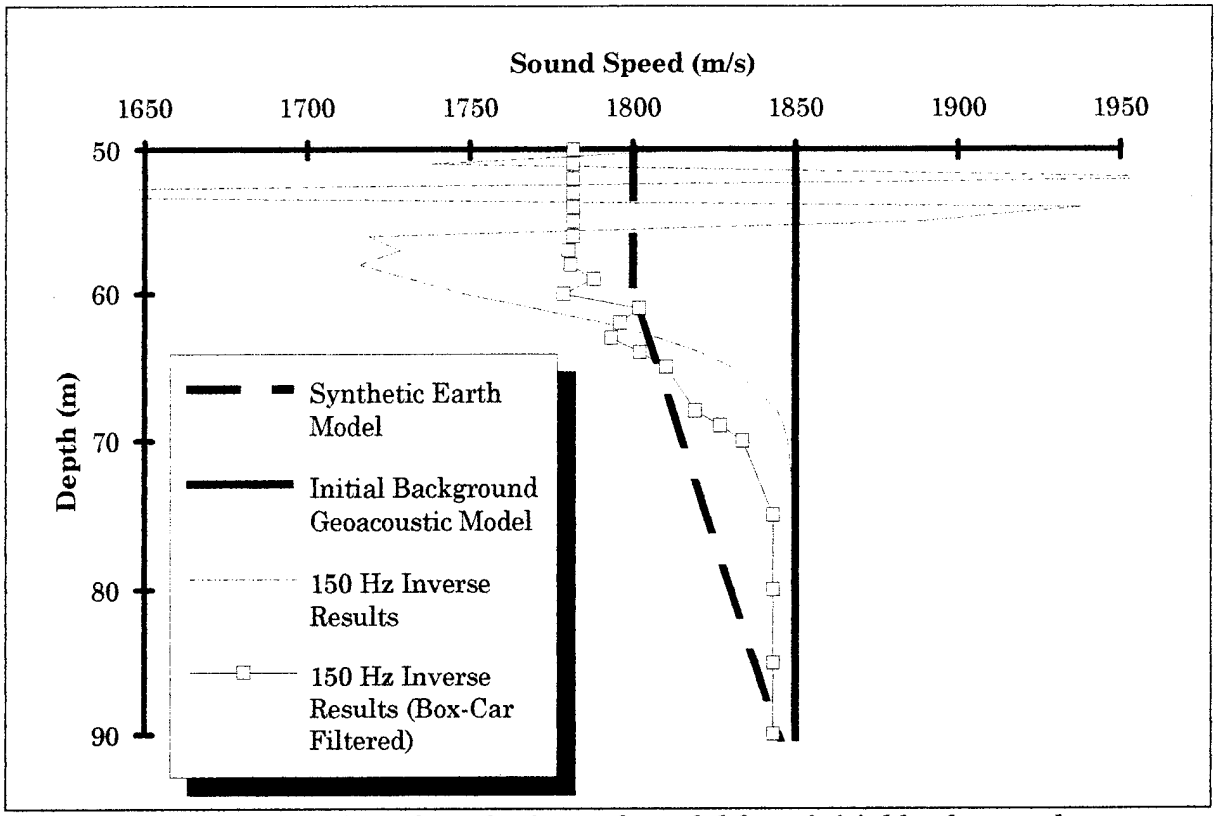

Figure 11. 150 Hz Inversion of synthetic earth model from initial background model B1.

As evident from the plots, the sound speed profiles are corrected in the proper direction relative to the background model. The profile in the upper tens of meters are lower in speed relative to the background, whereas the profile beyond about 90 m depth is virtually unaffected by the perturbation. Clearly, the 25 and 50 Hz signals correct the profile to greater depths than the 140 Hz signal. However, the 140 Hz signal approximates the sound speed at the water-bottom interface more accurately than the lower frequencies. Also apparent from the plots is that as the normal mode function decreases with depth, the inferred sound speed profile returns to the background profile.

Figures 12-14 show the results of recovering the synthetic earth model using the background model B2. The results are qualitatively the same as the previous background model B1. Even though the background

models differ significantly, the solutions converge about a sound speed profile which is strikingly similar to the synthetic earth model.

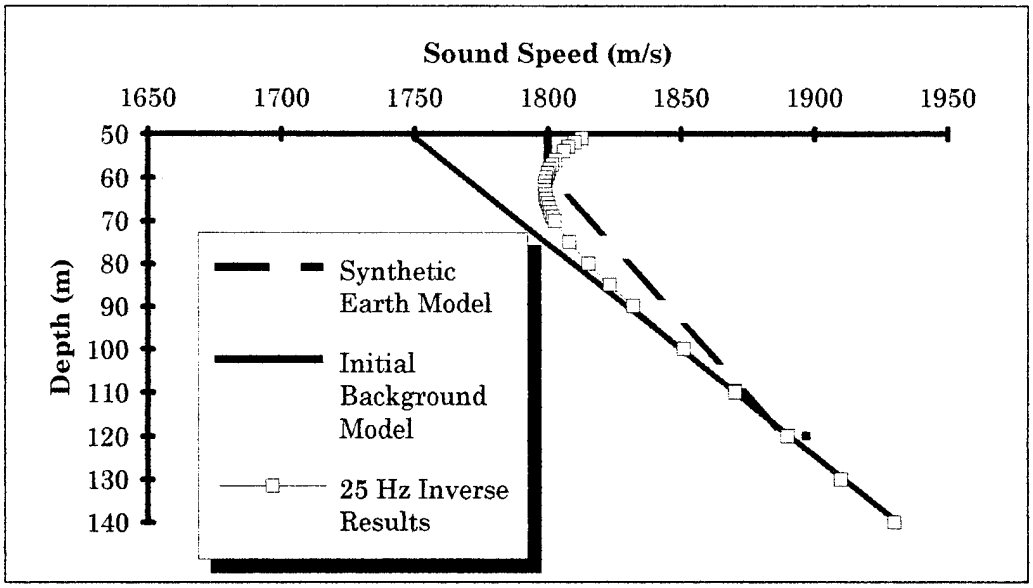

Figure 12. 25 Hz Inversion of synthetic earth model from background model B2.

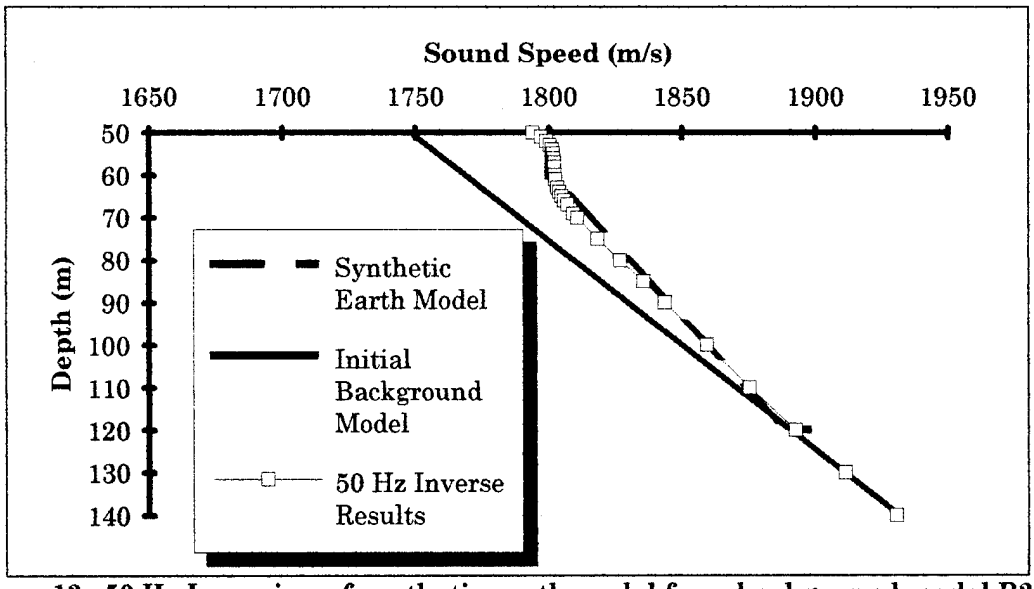

Figure 13. 50 Hz Inversion of synthetic earth model from background model B2.

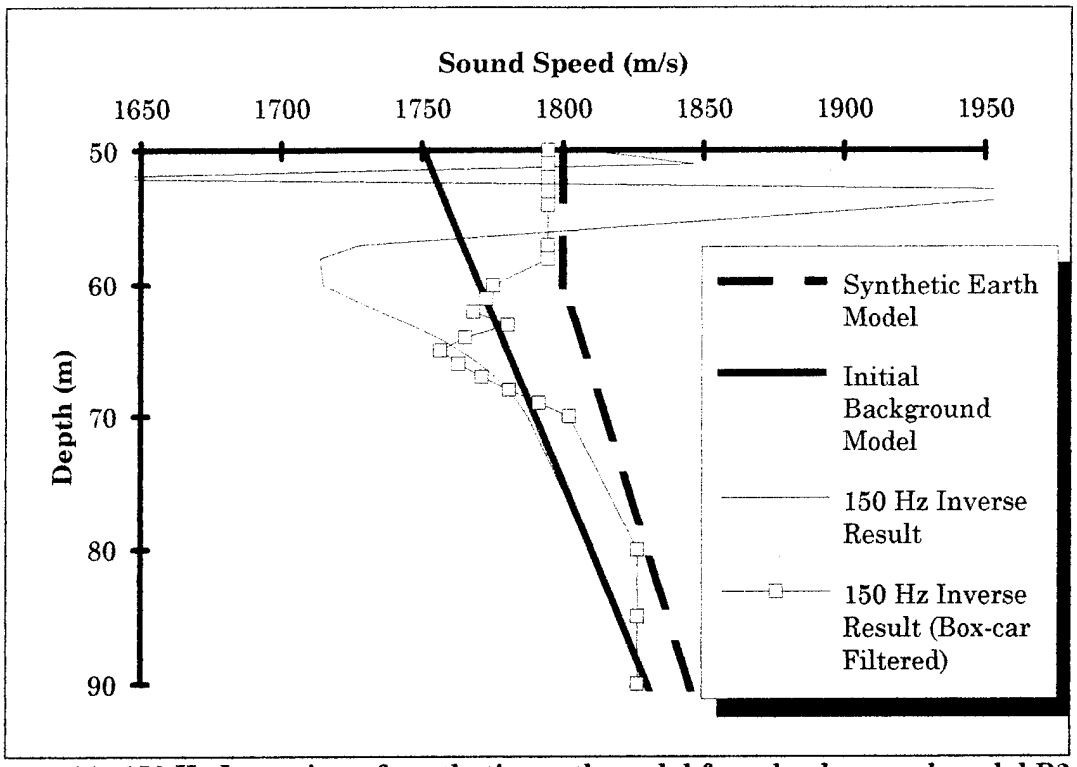

Figure 14. 150 Hz Inversion of synthetic earth model from background model B2.

The source angles in the data and the models are predominantly small (< 20°) and thus the perturbation technique alone can not be expected to resolve geoacoustic features much beyond an acoustic wavelength below the water-bottom interface. To resolve the deeper structures, a deep earth model algorithm based upon standard seismic (high source angle) signal processing techniques is presented in Section IV of this thesis. Since these methods are industry standard in the petroleum exploration industry, no attempt will be made to evaluate these techniques. However, the deep earth algorithm must be considered an essential part of the overall algorithm for Navy practical applications.

III. ACOUSTIC DATA / MODEL SUMMARY

A. EXPERIMENTAL OVERVIEW OF PROJECT GEMINI

A series of five shallow water, synthetic aperture array experiments collectively called Project GEMINI, were collected off of Corpus Christi, Texas in the fall of 1985. For the purpose of this thesis, only those measurements made at the shallow and deep sites will be discussed. The third site (Rubano site) has been studied extensively by previous efforts and a well defined geoacoustic characterization for the location is described in Matthews et al., 1985 and Rubano, 1980. A recent analysis of the GEMINI region by Duarte (1994) shows relatively good agreement between measured and modeled transmission loss quantities at the Rubano site. Given the relatively benign environment of the GEMINI region and the close proximity of the array sites, it was speculated by Duarte (1994) that the geoacoustic model, initially developed for the Rubano site, could be successfully used at the other two sites. However, he concluded that the TL data is particularly sensitive to the input geoacoustic parameters and that site-specific geoacoustic models are required in even in a benign, nearly range independent environment.

B. ENVIRONMENTAL DESCRIPTION OF THE GEMINI AREA

1. Sound Speed Profile

With the exception of the shallow site, CTD and XBT casts were made at the commencement and completion of each tow leg. Two weeks prior to the experiment, Hurricane Elena swept through the Gulf of Mexico and, as a result, established a well-mixed water column in the GEMINI region. Figures 15 and 16 show the sound speed profiles for the shallow and deep water sites, respectively. The sound speed profile for the shallow site (Figure 15) indicates isothermal conditions over the entire water column.

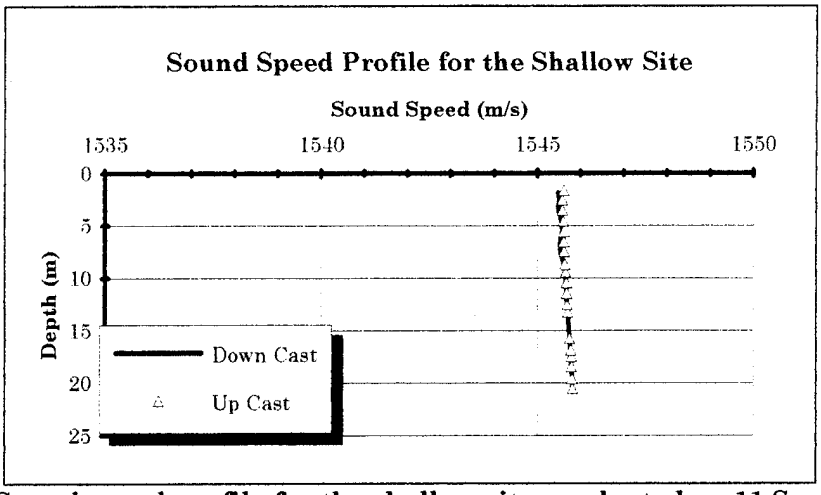

Figure 15. Sound speed profile for the shallow site conducted on 11 September 1985.

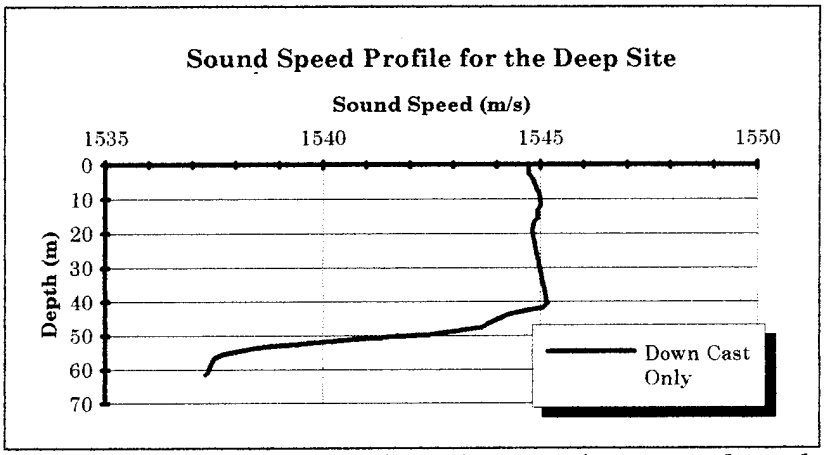

Figure 16. Sound speed profile for the deep site experiment conducted on 12 September 1985.

The sound speed profile for the deep site (Figure 16) also shows the presence of a near isothermal water column down to about 41 m overlying a low sound speed layer of approximately 10 m in thickness. This results in a thermocline gradient of approximately $-0.7084\ s^{-1}$. This negative sound speed gradient causes sound rays to refract downward and thus accentuate sound propagation in the sub-bottom.

2. Bathymetry

The Texas continental shelf is characterized by relatively smooth topography which gently dips toward the southeast. During Project GEMINI high resolution bathymetric data were collected along each of the propagation paths as well as at each of the station locations. Bathymetry versus range from the array locations are shown in Table 5. Each of the tow legs of the experiment was approximately 5000 m in length thus giving an average bottom slope at the shallow site of approximately 0.011° and about 0.054° for the deep site.

Bathymetry at the Shallow Site		Bathymetry at the Deep Site	
Range (m)	Depth (m)	Range (m)	Depth (m)
0	21	0	62
543	21	767	61
2288	21	1441	61
3783	20	2255	60
5460	19	3425	60
		4123	58
		4974	58

Table 5. Bathymetry for the GEMINI track experiments versus range.

C. GEOACOUSTIC MODELS FOR THE GEMINI REGION

1. Background

In order to compare the measured TL to the SNAP and FEPE model estimates of TL, geoacoustic models were constructed at the shallow and deep water sites. A geoacoustic model describes the depth dependence of compressional and shear wave speeds, compressional and shear wave attenuation, and density for each layer in the seafloor. In general, a geoacoustic model defines the true thicknesses and properties of the sediment and rock layers in the sea floor. Since a geoacoustic model only represents

the physical properties at a single point, multiple data sets must be formed to account for the variations in sediment properties in the horizontal.

In a recent analysis of TL in the GEMINI area, Duarte (1994) showed that even in a near range-independent environment such as the GEMINI area, model TL fluctuations are site specific and highly dependent on the input geoacoustic parameters. Moreover, he found that TL data and model comparisons were in good agreement at the Rubano site where a site specific geoacoustic model was developed and incorporated into the propagation models. At the shallow and deep sites the Rubano geoacoustic data were used in the model calculations and rather poor agreement resulted. Thus, it appears that geoacoustic data obtained for one location can not be used at sites just 12 nm away, even in a seemingly range-independent environment. Because of this horizontal variability, it was then necessary to construct geoacoustic models for the shallow and deep sites of the GEMINI region. These are discussed in the next section.

2. Regional Geology

Glaciation during the Pleistocene era, 0.012-2.8 million years before present (mybp), created recognizable imprints on Gulf of Mexico sedimentation patterns. Table 6 is a generalized geologic time scale for reference. With the growth and subsequent retreat of the ice sheets, sea level fell (regressed) and rose (transgressed) accordingly. During the regressive sequences, numerous stream channels appeared along the present-day Texas continental shelf. Lowering sea levels caused rapid seaward progradation of river deltas, which rapidly expanded the continental margins. During transgressive sequences, when mean sea-level rose, vast areas of the former coastline were submerged. The stream channels which once occupied the continental shelf regions were subsequently filled with fine-grain sedimentary deposits.

Period	Epoch	Glacial Stage	Sea Level	Time
	Holocene		Transgression	0.012 mybp
		Late Wisconsin	Regression	
		Mid Wisconsin	Transgression	0.1 mybp
		Early Wisconsin	Regression	
		Sangamon	Transgression	
Quaternary		Late Illinoian	Regression	
	Pleistocene	Mid Illinoian	Transgression	
		Yarmouth	Transgression	
		Kansan	Regression	2.1 mybp
		Aftonian	Transgression	
		Nebraskan	Regression	2.8 mybp
	Pliocene			
Tertiary				5.2 mybp

Table 6. Geologic time scale for the Quaternary Period (From Matthews et al., 1985).

The Holocene age sediment layer represents the last transgressive sequence in the post-glacial period. This sequence is characterized by fine grain silty-clays and represents the uppermost, surficial sediments in the GEMINI region. A thorough discussion of the sediment properties for the Holocene sequence is presented in Matthews et al. (1985). The thickness of the Holocene layer varies substantially in the GEMINI region. An isopach chart of the Holocene age sediments is shown in Figure 17 (Berryhill and Tippet, 1981). In general, the Holocene layer thickens seaward as evident by the seaward increase in two-way travel time from 10 to 40 ms. The dashed lines on the chart represent the more prominent relict stream channels along the shelf. The presence of stream channels on multi-channel seismic profiles is one means of discerning the interface between Holocene age sediments and the underlying late Wisconsin sedimentary sequence (Matthews et al., 1985). Since these stream channels were later filled by post-Wisconsin age sediments, the Holocene age sequences are thicker in these localized regions (in excess of 12 m) than in the surrounding Holocene silty-clay layers.

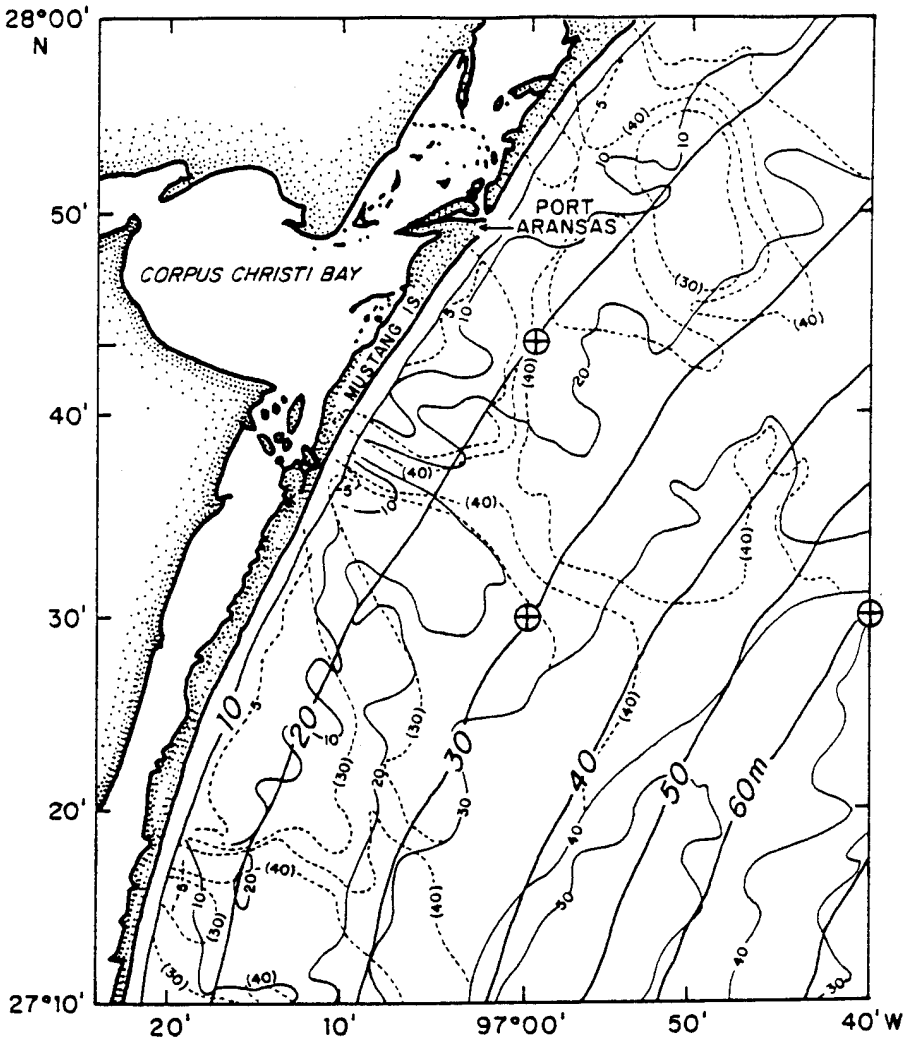

Figure 17. Sediment isopach chart of the GEMINI region expressed in milliseconds of two way travel time (broad solid line). Narrow solid line represents sediment deposited since the last low stand of sea level. Dashed lines represent the outline of localized thicker accumulations of sediment in ancient stream channels. One millisecond is approximately equal to 0.73 m (Berryhill, 1981). GEMINI array locations are denoted by the ⊕ symbol.

The U. S. Naval Oceanographic Office (NAVOCEANO) in conjunction with ARL/PSU collected 16 gravity cores in the GEMINI region (Ross et al., 1978). The results of their analysis indicates that the Holocene age silty-clay layer has a mean density of 1.557 g/cm^3 and an average sound speed ratio (i.e., ratio of sediment sound speed to bottom water sound speed) of 0.987. These values differ slightly from the generic values presented in Hamilton (1980) for continental shelf and slope environments. However, the Ross et al.

data represents site-specific conditions and as such are preferred for use in the geoacoustic models. Unfortunately, none of the cores were able to extend deep enough to sample the underlying late-Wisconsin layers. Matthews et al, (1985) interprets this layer to be a very fine sand or sandy silt. Based upon the shallow water sediment tables of Hamilton (1980), the late-Wisconsin sediments are assumed to have a density of 1.77 g/cm^3 and a sound speed ratio of 1.080.

Figure 18 is a representative seismic profile (east-west transect) for the GEMINI region. As evident from the figure, the seismic sequence is characterized by gently sloping, nearly parallel reflectors broken up by intermittent growth faults and stream channels. The strong reflection pattern occurring at the Holocene-late Wisconsin interface is indicative of the strong impedance contrast across the interface. Since acoustic impedance is the product of a material's density and sound speed, a strong reflection

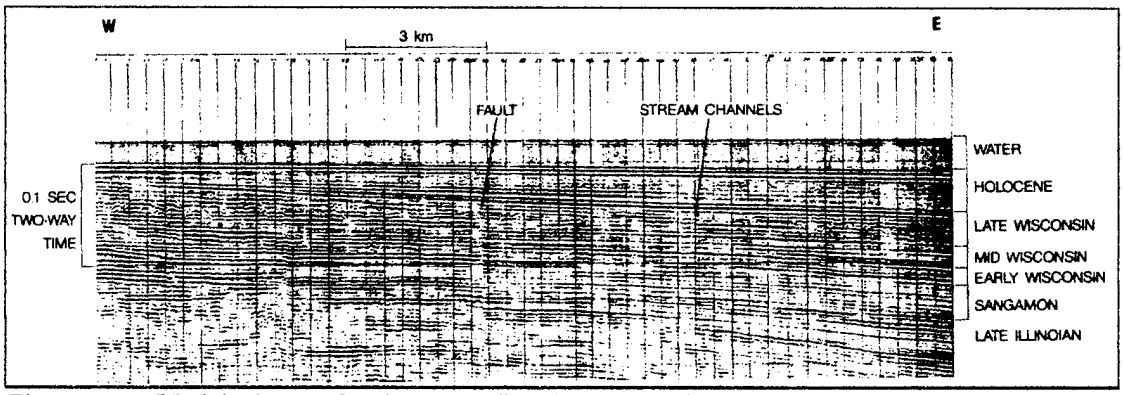

Figure 18. Multi-channel seismic reflection record across the Texas continental shelf near Corpus Christi. A relict stream channel from the Late Wisconsin transgression is shown.

pattern on a seismic profile normally suggests a large change in lithology across an interface. The Holocene silty-clay layer is characterized by a relatively low sound speed and density whereas the late Wisconsin sandy silt layer is characterized by a much greater sound speed and density values.

This impedance contrast supports the well-defined layering structure in Figure 18.

3. Geoacoustic Model Development

Both the shallow and deep water sites have environmental and acoustic propagation characteristics similar to the Rubano site which was previously reported in Matthews et al. (1985) The sites differ only in water depth and in the thickness of the Holocene age sedimentary sequence. Minor differences in water column sound speed are also apparent, however these variations do not significantly impact the geoacoustic characterizations The shallow site is situated in about 20.5 m of water and the underlying Holocene-age silty clay layer is estimated to be 8 m thick. The deep site is situated in about 63 m of water. At the deep site the Holocene layer is estimated to be about 24 m thick.

At each site the sound speed ratio for the silty-clay layer is assumed to be 0.987, which implies that the sound speed of the silty-clay layer is less that the overlying water column. Using methods described in Hamilton (1980), the compressional wave speed expressed as a function of depth takes the form of the following regression formula:

$$V_p = V_{bw}\,(0.987) + 1.3\ s^{-1}(Z) \qquad (46)$$

where V_p is the compressional wave speed in m/s, V_{bw} is the bottom water sound speed in m/s, and Z is the depth of sedimentary layer below the seafloor. The product $V_{bw}(0.987)$ represents the initial sound speed (V_o) of the sediment. The sediment sound speed gradient (1.3 s^{-1}) was established from the NAVOCEANO cores and is consistent with the near-surface sound speed gradients reported in Hamilton (1979). Because the thickness of the Holocene sediments does not exceed a few tens of meters, the higher order terms of Equation (46) (not shown) make negligible contributions to the sound speed profile in the sediment layer and therefore are neglected

(Matthews et al., 1985). As a result, the compressional wave speed in the Holocene layer can be expressed as a linear function of depth.

Thermal variations at the sea floor can have a pronounced effect on the upper sediment layer sound speed gradient. If a periodic thermal fluctuation is applied at the water-sediment interface, a thermal wave will propagate into the sediment. The depth to which the temperature effects will be felt is dependent on the sediment thermal conductivity and the heat flow (Matthews et al., 1985). In a study of the seasonal variation of compressional sound speed due to temperature variability in the water column, Rajan et al. (1992) showed that this depth of influence was about 3 m below the water-sediment interface. Therefore, to account for the thermal variability at the seafloor, Matthews et al. (1985) imposed a negative sound speed gradient in the upper 2.5 m of the Holocene layer. Below this depth the sound speed profile follows that expressed in Equation (46).

The late-Wisconsin sediments can be modeled in a similar fashion. Based upon the shallow-water sediment tables of Hamilton (1980), these sediments are interpreted to have a sound speed ratio and density of 1.080 and 1.77 g/cm^3, respectively. In general, fine grained sands are characterized by large sound speed gradients near the surface decreasing sharply with depth (Hamilton, 1980). As a result, the sound speed profile as a function of depth is curve-linear.

$$V_p = 1681\, Z^{0.013} \qquad (47)$$

The sound speed constant in Equation (47) is based on sediment values at the water-sediment interface. For a buried layer, such as the late Wisconsin sand, compensation must be made for the lithostatic load from the overlying Holocene sediments. Initial values of compressional wave speed for the late Wisconsin layer are estimated by matching the lithostatic load corresponding to the overlying Holocene sediments to a similar lithostatic load at depth in the late Wisconsin sediment layer. At the shallow site the

compressional wave speed at the top of the late Wisconsin sediment layer is estimated to be 1717.9 m/s. For the deep site, with the increased overburden pressure, the compressional wave speed increases to a value of 1731.0 m/s. Figure 19 illustrates the sound speed profiles through the different lithofacies for the shallow and deep sites. Of particular interest in these profiles is the relative thicknesses of each propagating media. The thickness of the Holocene sequence more than doubles in thickness between the shallow and deep sites. As will be shown later, this causes significant fluctuations in the TL versus range curves.

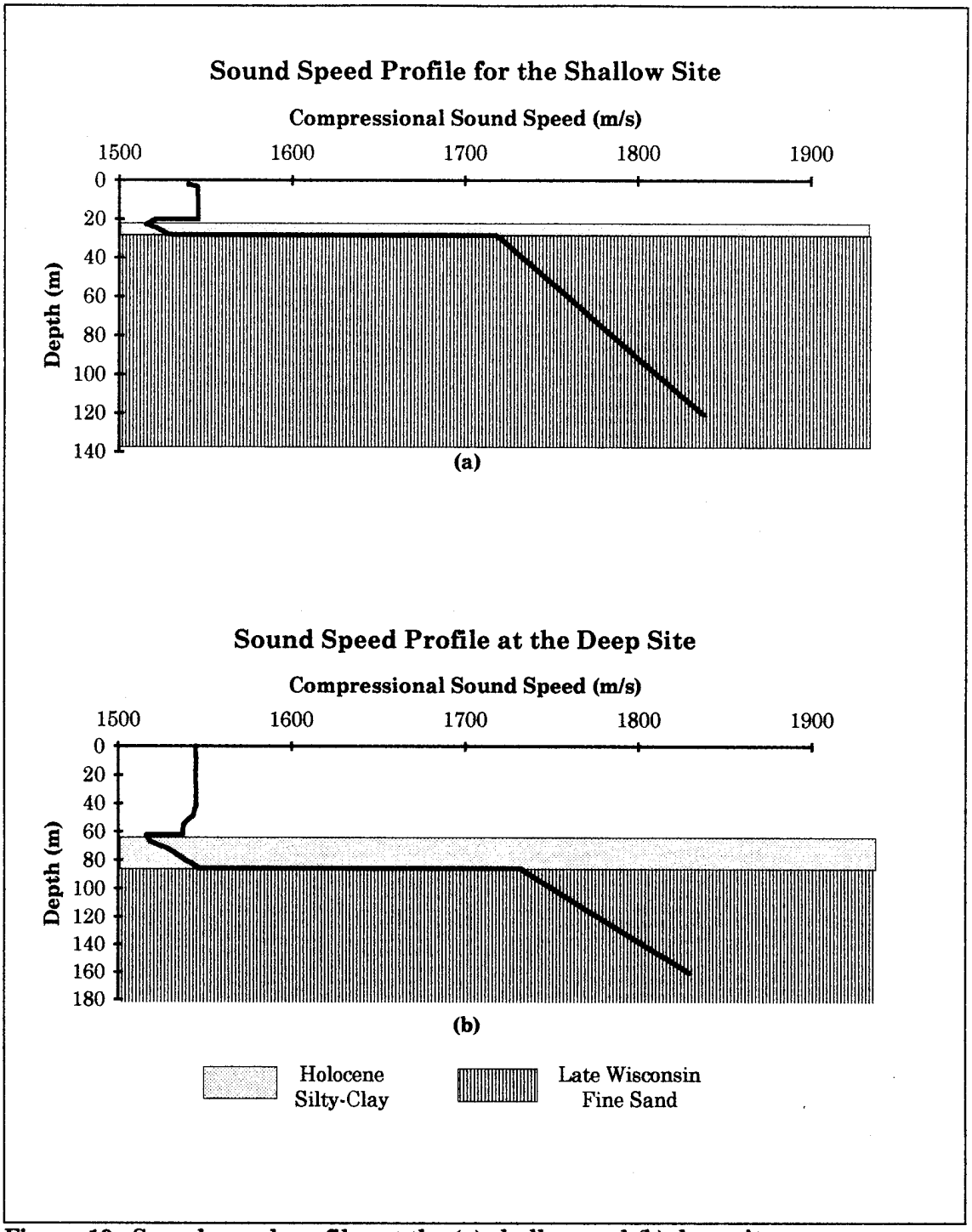

Figure 19. Sound speed profiles at the (a) shallow and (b) deep sites.

For terrigenous silty-clay sediments Hamilton (1978) showed that the sediment bulk density varies linearly as a function of compressional wave speed for the first few hundred meters below the sea floor. For the

Holocene layer, sediment density as a function of compressional wave speed was computed using the equation:

$$\rho = 1.135(V_p(Z)) - 0.155 \qquad (48)$$

Here the regression constant (0.155) was adjusted in the equation to match the mean surface density of the 16 cores collected by NAVOCEANO. For the late Wisconsin sequence, sediment density as a function of compressional wave speed is expressed as:

$$\rho = 1.1175(V_p) - 0.1245 \qquad (49)$$

Since there were no cores which penetrated into this layer, the density structure is speculative and is based on historical trends from Hamilton (1979).

Current estimates of low-frequency compressional wave attenuation have generated much debate in the acoustic community. Hamilton (1972) reported the results of *in situ* measurements of compressional wave speed and attenuation in various sediments off San Diego. These measurements and others from the literature allowed for analyses of the relationships between attenuation and frequency and other physical parameters to be made. Three important relationships resulted from the analyses: (1) compressional wave attenuation in marine sediments is approximately related to the first power of frequency in sands, muds, and sedimentary rocks, (2) attenuation can be estimated from sediment grain size (porosity) data, and (3) attenuation in marine sediments typically increases with depth due to the reduction of sediment porosity to a point where overburden pressure becomes the dominant effect. Beyond this null point, attenuation decreases smoothly with depth and overburden pressure (Hamilton, 1976).

Using the methods proposed in Hamilton (1976), the linear relationship between compressional wave attenuation and frequency takes the form

$$\alpha = K_p f^n \qquad (50)$$

where α is the attenuation of compressional waves in dB/m, K_p is the attenuation in dB/m-kHz, f is the frequency in kHz, and n is the exponent of frequency (assumed to be 1). The proportionality constant K_p at the water-sediment interface is estimated from the sediment porosity and mean grain size. According to Hamilton (1980), shallow water silty-clay sediments have an average porosity and mean grain size (in phi units) of 75.9% and 8.52ϕ, respectively. These values result in an estimate of attenuation at the water-sediment interface which is an order of magnitude greater than published attenuation results of Mitchell and Focke (1980). Matthews et al. (1985) chose to use values for sediment porosity and mean grain size between those predicted for shallow-water sediments by Hamilton and those values indicated by Mitchell and Focke. As a result, the lower error bar estimate for an 8.0ϕ particle was used to determine the proportionality constant. This yielded an attenuation value of 0.03 dB/m-kHz at the water-sediment interface. An expression relating the compressional wave attenuation for the Holocene silty-clay layer as a function of depth can thus be written as:

$$K_p = 0.030 + 0.0016(Z) \qquad (51)$$

The attenuation gradient (0.0016 dB/m^2-kHz) was established in Matthews et al. (1985) and is consistent with attenuation gradients reported in Hamilton (1976) for silty-clays

Compressional wave attenuation for the late Wisconsin sand layer, can also be empirically related to grain size and porosity. In general, sound attenuation for sands are much larger than those of silts, clays, and

muds (Hamilton, 1976). For sands, sound attenuation decreases with depth and increasing overburden pressure. For the late Wisconsin sequence, the attenuation profile is calculated from the following equation from Matthews et al. (1985):

$$K_p = 0.29930 - 0.00067(Z) \qquad (52)$$

Even though the Holocene and late Wisconsin age sediments possess enough dynamic rigidity to support shear wave propagation, shear wave speed and attenuation were not incorporated in the acoustic models. Given the shallow water depths, the relatively thin sediment cover, and the low frequencies involved at the GEMINI region, shear wave production was assumed to make a negligible contribution to the overall acoustic field (Rajan, 1994).

Geoacoustic model tabulations for the shallow and deep water sites are listed in Tables 7 and 8, respectively. As previously discussed, the models consist of an upper sequence of Holocene age silty-clays overlying a late-Wisconsin age fine sand sequence.

Material	Depth (m)	Sound Speed Vp (m/s)	Density (g/cc)	Sound Attenuation Kp (dB/m-kHz)
Sea Surface	0.00	1531.93	1.00	0.000
	1.80	1531.96	1.00	0.000
	2.40	1539.96	1.00	0.000
	3.40	1545.48	1.00	0.000
	4.50	1545.56	1.00	0.000
	5.50	1545.58	1.00	0.000
	6.60	1545.53	1.00	0.000
	7.70	1545.55	1.00	0.000
	8.70	1545.63	1.00	0.000
Water	9.40	1545.65	1.00	0.000
Column	10.40	1545.67	1.00	0.000
	11.60	1545.68	1.00	0.000
	12.60	1545.69	1.00	0.000
	13.20	1545.71	1.00	0.000
	15.40	1545.75	1.00	0.000
	16.70	1545.76	1.00	0.000
	17.70	1545.77	1.00	0.000
	18.60	1545.8	1.00	0.000
	19.60	1545.81	1.00	0.000
Water-Sediment Interface	20.50	1545.82	1.00	0.000
	20.51	1520.75	1.57	0.030
Holocene Age	23.00	1515.75	1.56	0.032
Silty-Clay	25.50	1523.25	1.57	0.030
	28.00	1528.25	1.58	0.036
	28.48	1531.13	1.58	0.030
	28.49	1717.93	1.79	0.296
	30.50	1721.18	1.80	0.293
	35.50	1727.68	1.81	0.292
	40.50	1734.18	1.81	0.289
	45.50	1740.68	1.82	0.286
	50.50	1747.18	1.83	0.284
	55.50	1753.68	1.84	0.281
	60.50	1760.18	1.84	0.279
	65.50	1766.68	1.85	0.276
	70.50	1773.18	1.86	0.274
Late Wisconsin Age	75.50	1779.68	1.86	0.272
Fine Sand	80.50	1786.18	1.87	0.269
	85.50	1792.69	1.88	0.267
	90.50	1799.18	1.88	0.265
	95.50	1805.68	1.89	0.263
	100.50	1812.18	1.90	0.260
	105.50	1818.68	1.91	0.258
	110.50	1825.18	1.92	0.256
	115.50	1831.68	1.92	0.254
	120.50	1838.18	1.93	0.252

Table 7. Geoacoustic Model for the Shallow Water Site.

Material	Depth (m)	Sound Speed Vp (m/s)	Density (g/cc)	Sound Attenuation Kp (dB/m-kHz)
Sea Surface	0.00	1544.74	1.00	0.000
	1.70	1544.74	1.00	0.000
	2.50	1544.72	1.00	0.000
	3.60	1544.79	1.00	0.000
	4.40	1544.85	1.00	0.000
	5.60	1544.87	1.00	0.000
	6.50	1544.91	1.00	0.000
	7.40	1544.94	1.00	0.000
	8.70	1544.98	1.00	0.000
	9.40	1545.00	1.00	0.000
	10.70	1545.01	1.00	0.000
	11.70	1545.01	1.00	0.000
	12.70	1544.98	1.00	0.000
	13.20	1544.94	1.00	0.000
	15.60	1544.94	1.00	0.000
	16.50	1544.88	1.00	0.000
	17.50	1544.85	1.00	0.000
	18.70	1544.82	1.00	0.000
	19.60	1544.82	1.00	0.000
	20.60	1544.83	1.00	0.000
	21.60	1544.85	1.00	0.000
	22.50	1544.87	1.00	0.000
	23.60	1544.88	1.00	0.000
	25.60	1544.92	1.00	0.000
	26.70	1544.94	1.00	0.000
	27.90	1544.97	1.00	0.000
Water	28.40	1544.97	1.00	0.000
Column	30.70	1545.01	1.00	0.000
	31.70	1545.03	1.00	0.000
	32.60	1545.04	1.00	0.000
	35.50	1545.09	1.00	0.000
	36.10	1545.10	1.00	0.000
	37.40	1545.12	1.00	0.000
	38.40	1545.13	1.00	0.000
	39.40	1545.15	1.00	0.000
	40.40	1545.17	1.00	0.000
	43.70	1544.28	1.00	0.000
	46.50	1543.79	1.00	0.000
	47.50	1543.66	1.00	0.000
	49.70	1542.46	1.00	0.000
	50.50	1541.37	1.00	0.000
	51.60	1540.27	1.00	0.000
	52.50	1539.44	1.00	0.000
	53.50	1538.58	1.00	0.000

Table 8. Geoacoustic Model for the Deep Water Site

Material	Depth (m)	Sound Speed Vp (m/s)	Density (g/cc)	Sound Attenuation Kp (dB/m-kHz)
	54.60	1538.03	1.00	0.000
	55.60	1537.69	1.00	0.000
	56.70	1537.50	1.00	0.000
	57.60	1537.47	1.00	0.000
	58.60	1537.44	1.00	0.000
	59.00	1537.40	1.00	0.000
	60.30	1537.40	1.00	0.000
	61.50	1537.31	1.00	0.000
Water-Sediment Interface	62.34	1536.99	1.00	0.000
	62.35	1516.03	1.57	0.030
	67.34	1518.53	1.57	0.034
	69.84	1523.53	1.57	0.036
	72.34	1529.03	1.58	0.038
Holocene Age	74.34	1531.63	1.58	0.039
Silty-Clay	77.34	1535.53	1.59	0.041
	79.84	1538.78	1.59	0.043
	82.34	1542.03	1.60	0.045
	84.84	1545.28	1.60	0.046
	86.00	1546.97	1.60	0.047
	86.01	1732.07	1.81	0.289
	91.00	1738.60	1.82	0.287
	96.00	1745.13	1.83	0.284
	101.00	1751.66	1.83	0.282
	106.00	1758.20	1.84	0.280
	111.00	1764.73	1.85	0.277
Late Wisconsin Age	116.00	1771.26	1.85	0.275
Fine Sand	121.00	1777.79	1.86	0.273
	126.00	1784.33	1.87	0.270
	131.00	1790.86	1.88	0.268
	141.00	1803.93	1.89	0.263
	151.00	1816.99	1.91	0.259
	156.00	1823.52	1.91	0.256
	161.00	1830.06	1.92	0.254

Table 8. Geoacoustic Model for the Deep Water Site (continued).

D. TRANSMISSION LOSS MODELS

In order to qualitatively assess the accuracy of the geoacoustic models (derived in the previous section), estimates of TL using the geoacoustic models as input were compared with the measured GEMINI TL data. TL must be considered the measure of effectiveness (MOE) for the performance of the inverse technique developed in this thesis. If measured and modeled TL agree exactly for two different geoacoustic models, then the differences in

the geoacoustic parameters are considered acoustically indistinguishable for a given frequency.

The normal mode model (SNAP) and the finite element parabolic equation model (FEPE) were used in this portion of the analysis to quantitatively determine the impact of the perturbative technique to estimate of the geoacoustic model. The results of these comparisons are given in the next section.

For the inverse theory problem developed in this thesis the selection of the proper acoustic propagation model to use is critical to the success of the inversion. The central issue for this study is the inversion of geoacoustic propertied from measured TL data assuming little to no *a priori* geoacoustic information is available. Therefore, it is crucial to have an acoustic model that is sensitive to even small variations in geoacoustic properties so that when the model and data agree well, the geoacoustic parameters are estimated accurately.

Although, the GEMINI region was selected by the U. S. Navy by virtue of its seemingly range-independent environment, the geoacoustic properties were shown to be just the opposite. For this reason SNAP could not be used in the inverse problem because of its adiabatic assumption (i.e., not fully coupled). KRAKEN is similar to SNAP, except that it is a fully coupled normal mode model. KRAKEN was used to calculate and display the normal mode functions and eigenvalues (Z(m) and k_m) that are inputs to the kernel of the Fredholm integral in Equation (40). The FEPE model has shown excellent agreement in comparison with fully coupled normal mode models and because FEPE is more efficient to run, it was the principle model used to compare inverse results with the measured TL data.

E. TRANSMISSION LOSS MODEL/DATA COMPARISONS

The GEMINI experiments consisted of towing a narrow-band CW source at a fixed depth away from a pair of moored receivers (Lynch et al., 1991). An NRL J15-3 acoustic source with output tonals of 50 and 140.05 Hz was used during the course of the experiment. The source and receiver configuration is shown in Figure 20 and in Table 1. The combination of the two depth settings along with the two source frequencies allowed for 4 complex pressure field magnitudes versus range measurements to be collected at each site. The complex pressure field measurements were transformed into transmission loss (TL) by the relation

$$TL(r,z) = -20 \log \frac{|p(r,z)|}{|p_o|} \qquad (53)$$

where $p(r,z)$ is the pressure field at range r and p_o is the acoustic pressure field at 1 meter distance from the source. In this section the measured TL results from the shallow and deep sites are presented along with TL estimates from FEPE and SNAP.

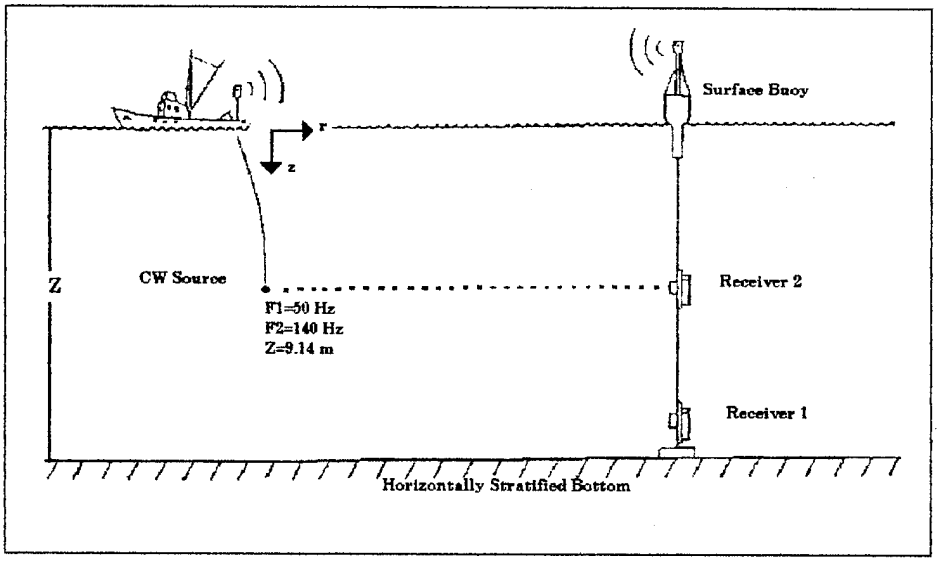

Figure 20. Experimental source and receiver configuration for the GEMINI experiments.

1. Shallow Site

The experimental TL measurements for the shallow site are illustrated in Figures 21-23 along with estimates of TL based upon SNAP and FEPE model estimates. The 50 Hz data reveal a predominantly two-mode interference pattern whereas the 140 Hz data show a more complicated, multi-mode interference pattern. The measured 50 Hz TL curve exhibits a high degree of attenuation attributed to a low compressional velocity layer in the sub-bottom. The curve also exhibits a high density of noise spikes beyond about 2500 m in range due to local seismic profiling activity in the region. These rapid fluctuations should be considered as artifacts in the data and are not expected to be modeled accurately.

Figures 21-23 illustrate the relatively close agreement between the measured and modeled TL estimates using as input the shallow site geoacoustic model. For the 50 Hz case (Figure 21a), beyond 2600 m there is a substantial increase in TL. As previously shown, the sediment thickness in the GEMINI region is highly variable. The sharp increase in TL is attributed to an abrupt increase in sediment thickness at about 2600 m in range. This feature is interpreted as one of the numerous late-Wisconsin age stream channels which criss-cross the Texas continental shelf (Matthews et al., 1985). This type of feature would account for this significant, localized increase in sediment thickness. To incorporate this range-dependency in the TL model estimates, a second geoacoustic model was developed for the shallow site. Based upon the sediment isopach chart (Figure 17), the Holocene age silty-clay layer was increased from about 8 m to 35 m in thickness. As evident from Figure 23, this range-dependent geoacoustic model improved the 50 Hz FEPE TL estimates for ranges beyond 2600 m. The 140 Hz signal (Figure 21b) was not significantly impacted by this range-dependency since most of the 140 Hz propagation occurs in the upper few meters of the sediment.

Overall, the FEPE TL estimates are more accurate than the SNAP TL measurements, a result that is in stark contrast to Duarte's (1994) conclusions regarding TL model for which he used the Rubano site geoacoustic data at the shallow site. Thus, it can be concluded that the shallow water TL model estimates are extremely sensitive to the geoacoustic model used. This conclusion is further illustrated by comparing the 140 Hz TL model results from the shallow site (Figure 21b) with those found in Duarte (1994) (Figure 24). The lone difference between the two FEPE model estimations rests with the input geoacoustic model used. As discussed earlier, the shallow site geoacoustic model consists of about 8 m of near surface, low-velocity sediments in contrast to 17 m at the Rubano site (Matthews et al., 1985). The thicker low-velocity sequence (Rubano model) results in more loss (>10 dB) than that experienced by using the shallow site geoacoustic model. The SNAP TL estimate also shows reasonably close agreement with the measured TL data.

Figures 21 through 23 suggest that the FEPE estimates of TL are in closer agreement with the measured TL field than those portrayed by SNAP. One possible reason for this is that SNAP is not a fully coupled normal mode model and, because the geoacoustic environment is range-dependent, the SNAP model does not permit energy to be exchanged between modes which the measured TL indicates is an important component.

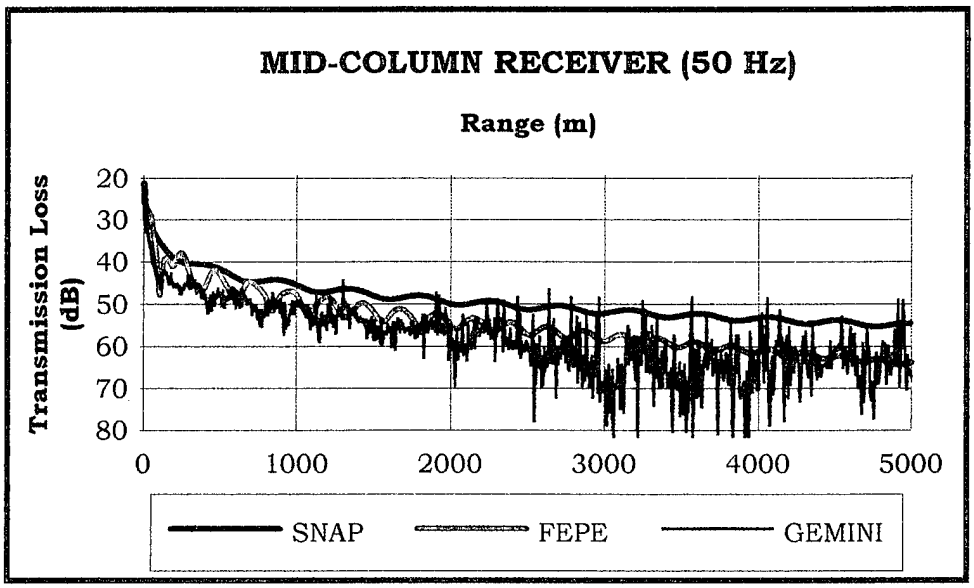

(a)

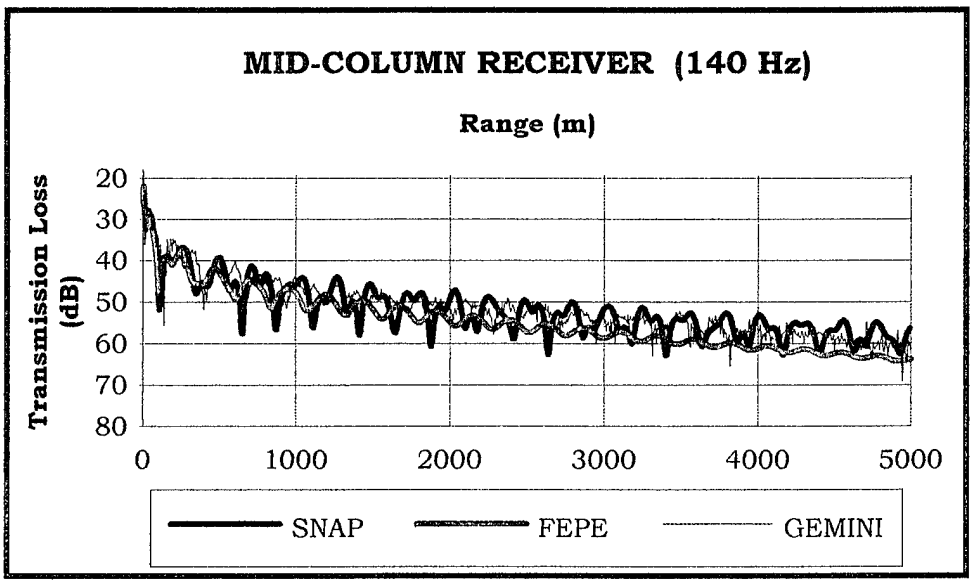

(b)

Figure 21. Comparison of experimental and theoretical transmission loss curves for the shallow site for a mid-column receiver. Frequency: 50 Hz (a), 140 Hz (b).

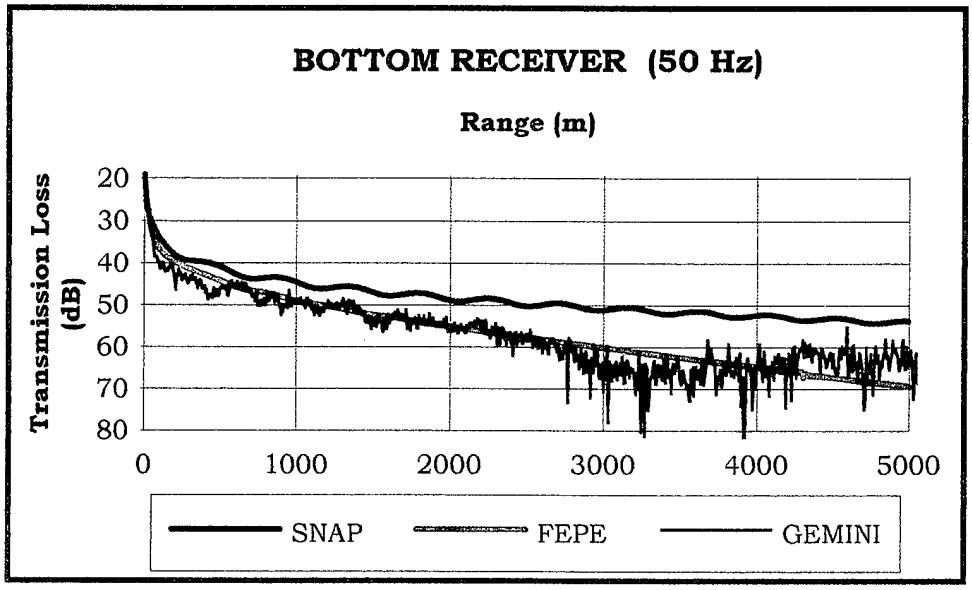

(a)

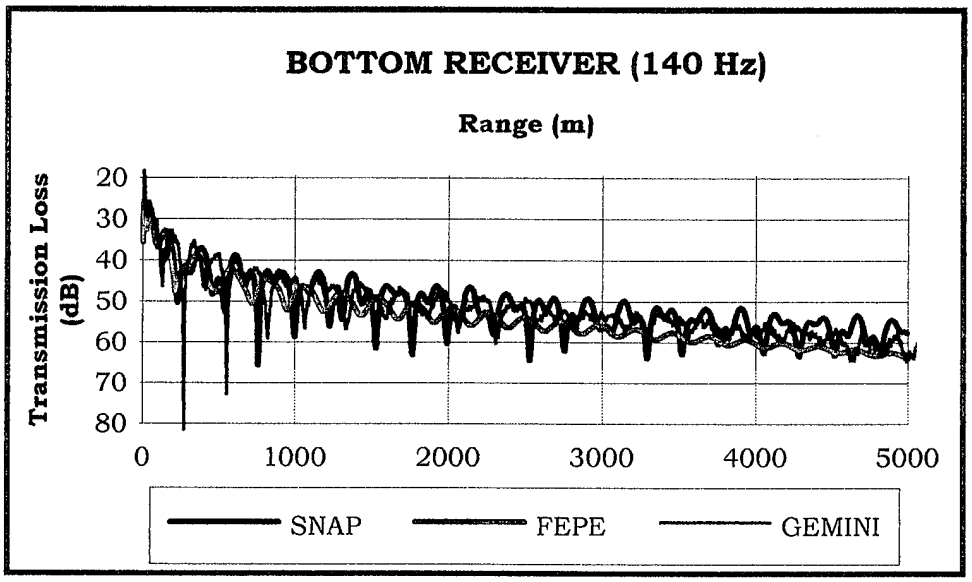

(b)

Figure 22. Comparison of experimental and theoretical transmission loss for the shallow site for a bottom receiver. Frequency: 50 Hz (a), 140 Hz (b).

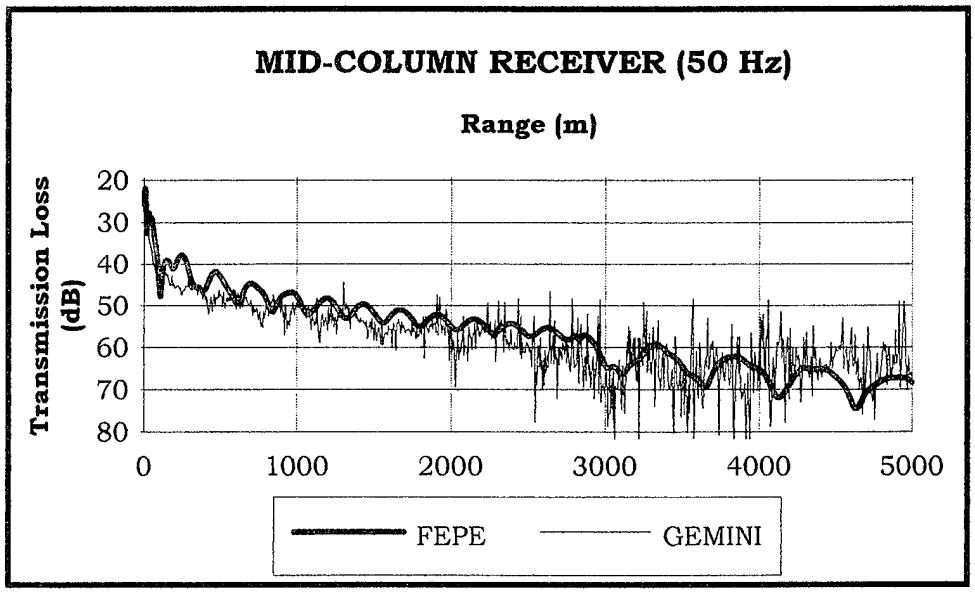

Figure 23. Plot of experimental GEMINI and range-dependent FEPE model transmission loss for the shallow site at 50 Hz.

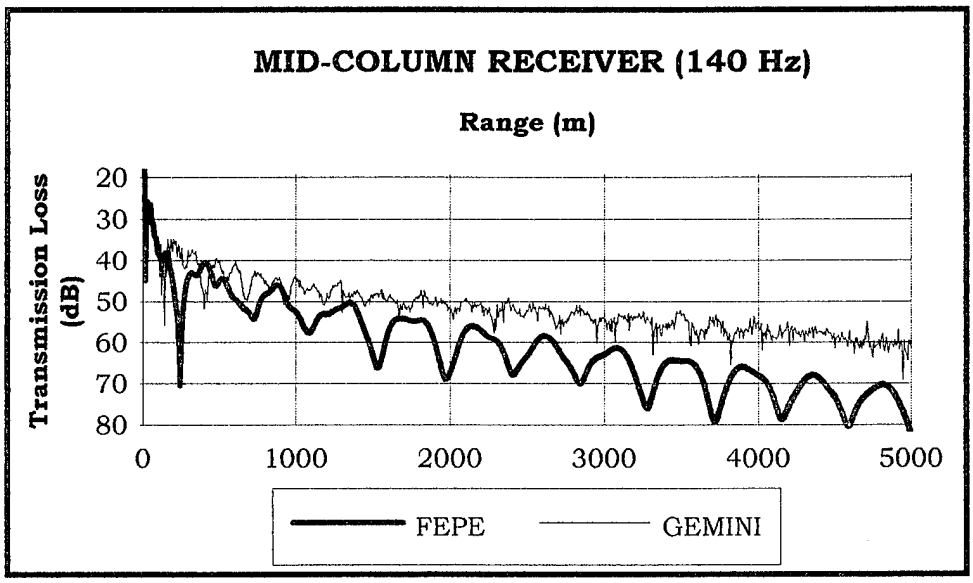

Figure 24. Comparison of GEMINI transmission loss data and FEPE transmission loss model estimates for the shallow site based upon the Rubano site geoacoustic model as input (Duarte, 1994).

2. Deep Site

The deep site was occupied on two different occasions during Project GEMINI (10 and 12 September 1985). Because the data collected from 10 September are incomplete only the data collected on 12 September are used in this study. The experimental TL measurements for the site are illustrated in Figures 25-26 along with model estimates of TL. As with the shallow site data, the measured TL is characterized by a predominant two-mode interference pattern for the 50 Hz signal and a multi-mode interference pattern for the 140 Hz signal. The FEPE and SNAP model TL estimates used the deep site geoacoustic model developed in the preceding section as input. Unlike the shallow site, the propagation path at the deep site was treated as range-independent.

Although there is reasonably good agreement in amplitude between the modeled and measured TL levels for the 50 Hz signal, both FEPE and SNAP fail to accurately model the TL fluctuations at the deep site. The TL fluctuations (Figure 25a) in excess of 20 dB. These fluctuations may be due to interfering normal modes at the site (Duarte, 1994).

Somewhat better agreement is noted between the modeled and measured TL levels for the 140 Hz signal. The 140 Hz signal shows a more complicated multi-mode interference pattern. As illustrated in Figure 25b, TL fluctuations are on the order of 20 dB in TL.

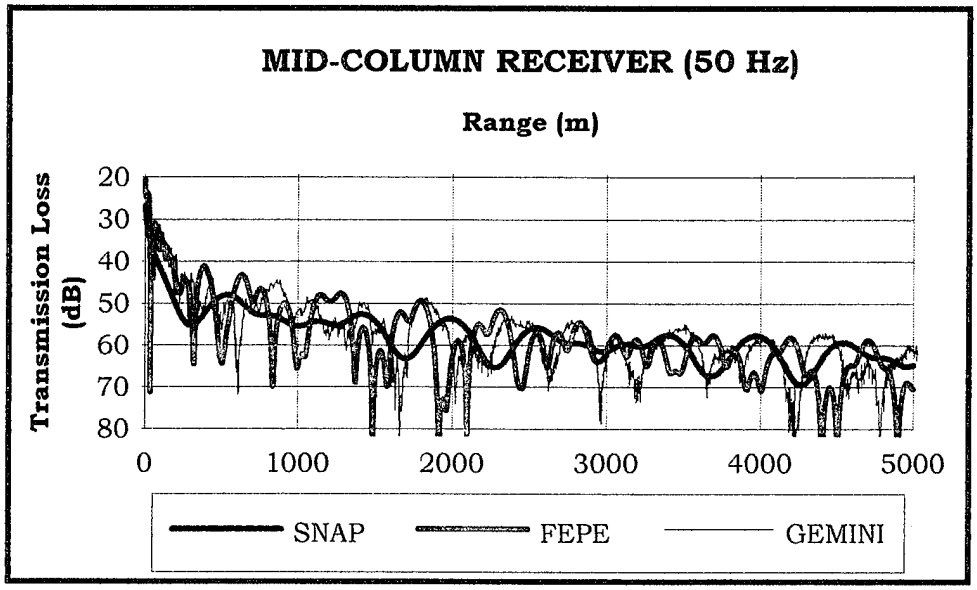

(a)

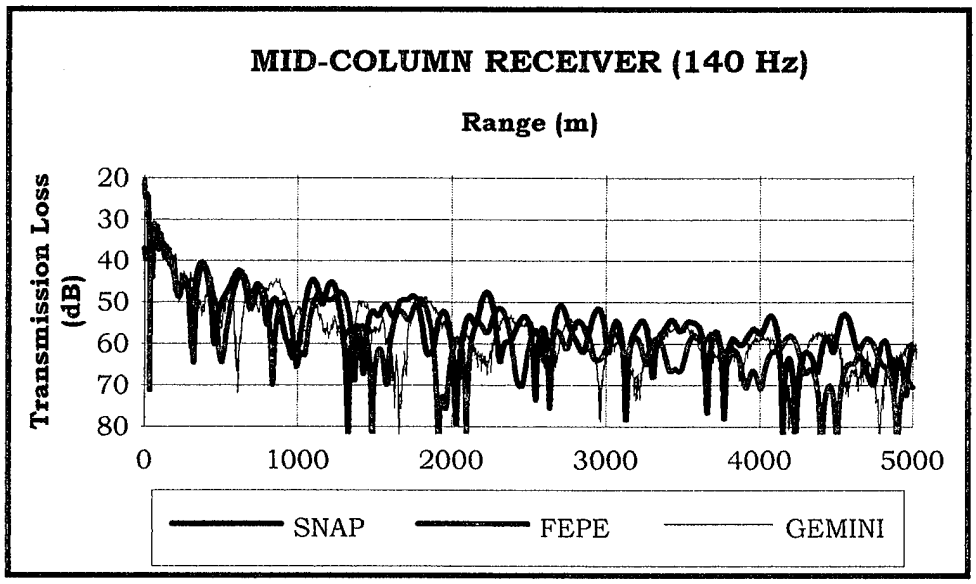

(b)

Figure 25. Comparison of experimental and theoretical transmission loss curves for 140 Hz for the deep site for the mid-column receiver. Frequency: 50 Hz (a), 140 Hz (b).

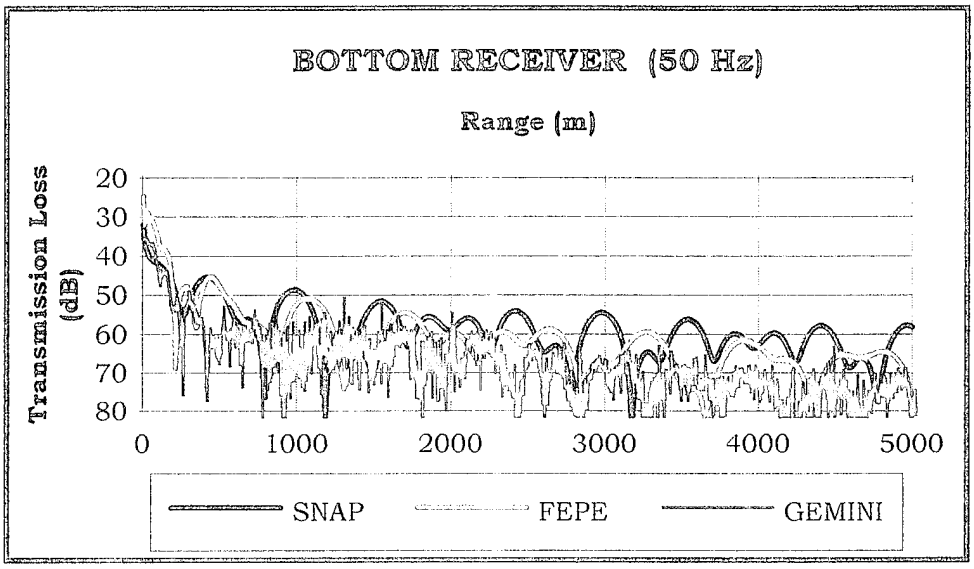

(a)

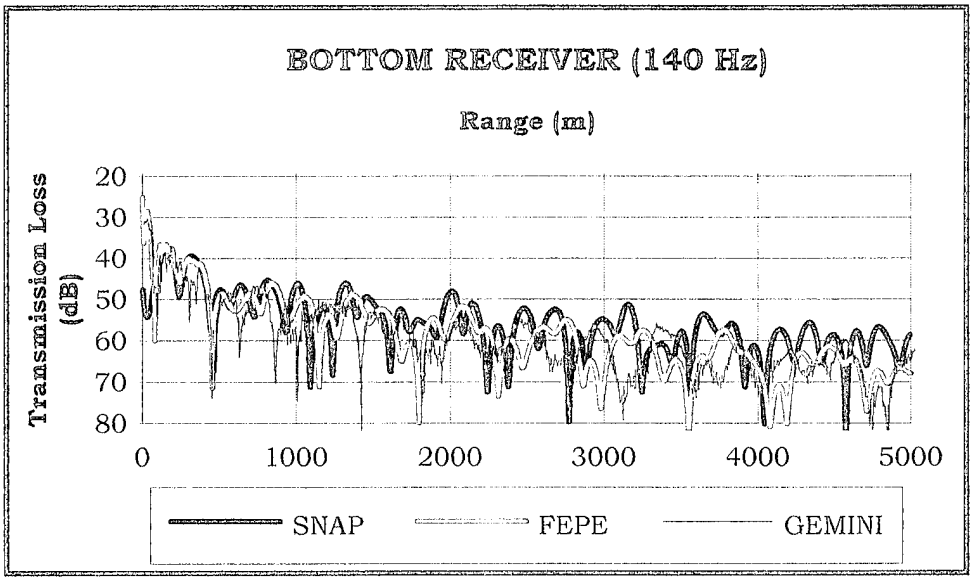

(b)

Figure 26. Comparison of experimental and theoretical transmission loss curves for 140 Hz for the deep site for the bottom receiver. Frequency: 50 Hz (a), 140 Hz (b).

IV. PERTURBATIVE INVERSION RESULTS

In this section the perturbative inversion technique is applied to the experimental data obtained during Project GEMINI. As a result of the inversion, a new set of geoacoustic parameters for the shallow and deep water sites are estimated. As discussed previously, TL is used as the measure of effectiveness of the inverse geoacoustic models. Since FEPE was shown to be more accurate than SNAP in estimating TL, only FEPE will be used in the comparison between measured and modeled TL values. The major strength of the inversion method is that *a priori* information of the sub-bottom is not required to estimate geoacoustic parameters. In order to demonstrate this, we assume that the geologic and geophysical properties of the environment are only vaguely known in the initial background geoacoustic models.

A. SHALLOW SITE

The results of Hankel transforming the experimental pressure field over the entire 5000 m range at 50 and 140 Hz are shown in Figure 27. Since the poles of the Green's function represent the eigenvalues for discrete modes for the particular waveguide at the given frequency, the location of these poles for the bottom receiver must be coincident with pole locations for the mid-column receiver. In this section only the plots for the bottom receiver are illustrated. However, in order to form an accurate estimate of the modal eigenvalues of the waveguide (k_{meas}), the results from the two receivers are averaged to form a single estimate for each frequency. The eigenvalues for the two frequencies are tabulated in Table 9. The 50 Hz plot (Figure 27a) shows one distinct peak at a horizontal wave number of about 0.19 m^{-1}. A less evident, very weak pole was found to be at a horizontal wavenumber of about 0.17 m^{-1}. For the 140 Hz case (Figure 27b), three trapped eigenvalues are readily identifiable from the plot.

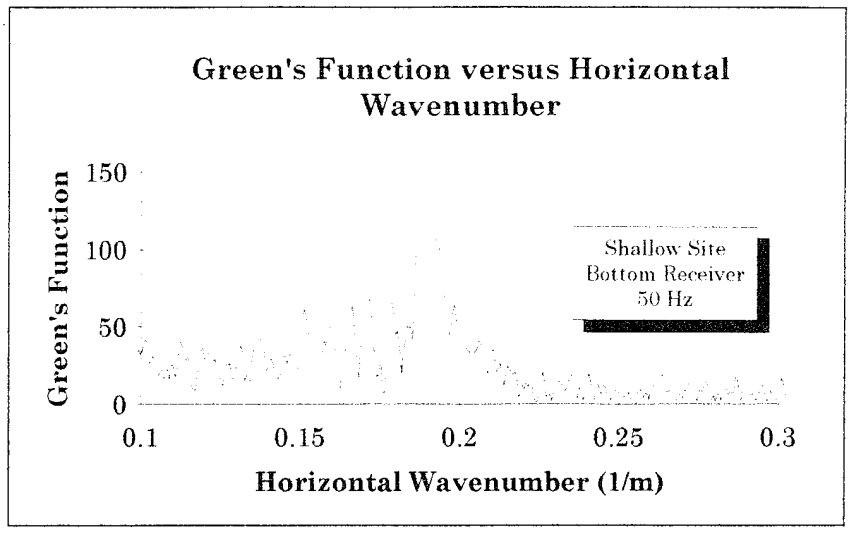

(a)

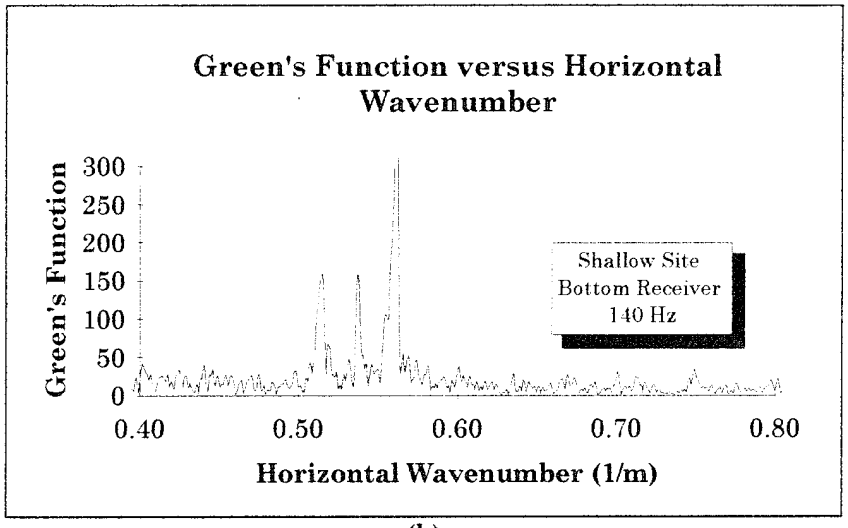

(b)

Figure 27. Magnitude of the depth dependent Green's function for the shallow site experiment. Frequency: 50 Hz (a), 140 Hz (b). Only the bottom receiver is shown.

Frequency (Hz)	Mode Number	k_{meas} (m^{-1})
50	1	0.1896861800
	2	0.1747074050
140	1	0.5541557518
	2	0.5431438446
	3	0.5201824925

Table 9. Measured mode eigenvalues for the shallow site.

Using the modes shown in Table 9, the pertubative inverse was performed separately for each frequency. In order to analyze the convergence of the inversion, two diverse initial background models were used in the inversion. The first background model, BG1, consisted of a constant gradient ($\nabla c = 2.0\ s^{-1}$) background profile with an initial sound speed of c(0) = 1500 m/s, and with a constant density of $\rho = 1.56\ g/cm^3$. The second background model, BG2, consisted of a constant gradient ($\nabla c = 1.25\ s^{-1}$) background profile with an initial sound speed of c(0)=1900 m/s and with a constant density of $\rho = 1.56\ g/cm^3$. Both background models used the experimentally measured sound speed profile of the water column in the inversion. The results of the 50 Hz inversion are displayed in Figure 28. Also shown as reference is the geoacoustic model developed in Section III.

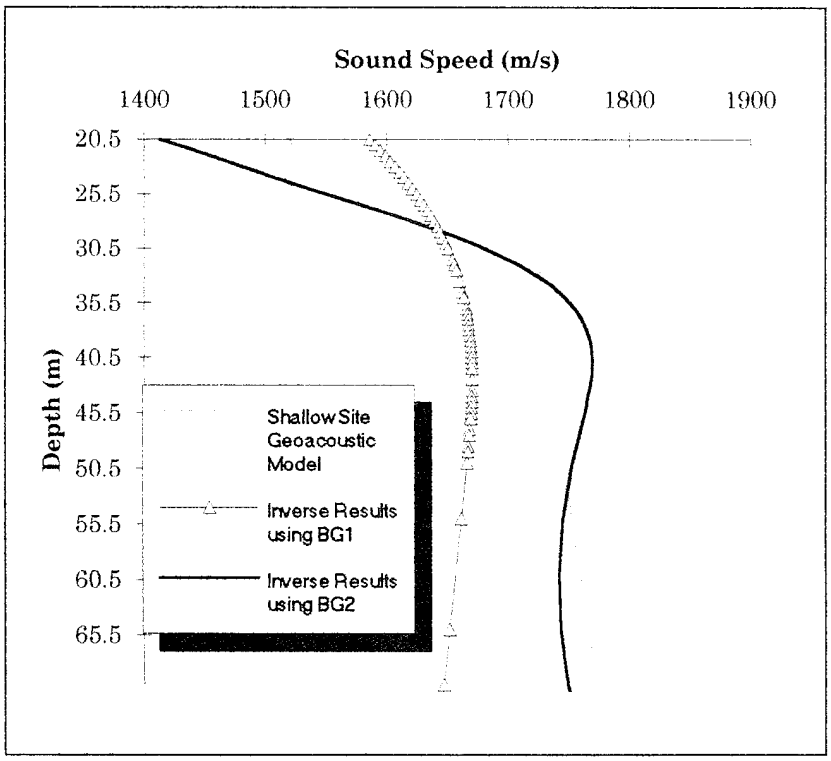

Figure 28. Results of the 50 Hz perturbative inversion using background models BG1 and BG2. The shallow site geoacoustic model derived in Section III is also shown.

Both profiles portray a lower sound speed sediment overlying a much higher speed geologic sequence. Even though there are similarities between the inverse results using BG1 and BG2, it is apparent that the inverse results of using BG2 as the background model are in closer agreement with the geoacoustic model than BG1. This effect suggests that the inversion process is highly dependent on the initial constraints of the background geoacoustic model used in the inversion. When this inversion algorithm can be automated, numerous initial estimates will be made and the conversion properties can be analyzed in more detail. If only a few initial estimates are made, the low eigenvalues can be used to assess stability of the inversion of the spectral decomposition in the Backus-Gilbert solution. The higher the magnitude of the low level eigenvalues, the more stable and accurate the solution.

Using the same initial background geoacoustic models, the results of recovering the sound speed profile for the 140 Hz signal are shown in Figure 29. As the number of modes and frequency increases, large fluctuation in c(z) result. To remedy this situation, a simple "box-car" average filter was applied to c(z). As with the 50 Hz case, the 140 Hz inversion suggests a two layer geologic sequence consisting of a lower speed layer overlying a higher speed layer.

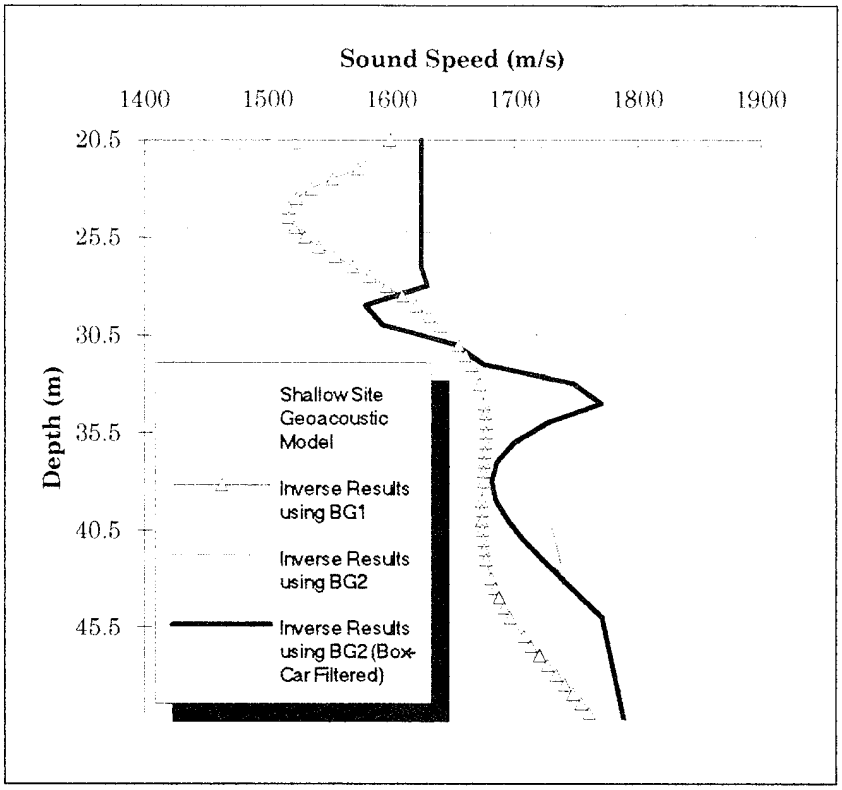

Figure 29. Results of the 140 Hz perturbative inversion using background models BG1 and BG2. The shallow site geoacoustic model derived in Section III is also shown.

It is important to emphasize that the inversion process did not incorporate any *a priori* information of the geologic and geophysical parameters of the seafloor. Geophysical parameters such as sediment density and compressional attenuation were held constant throughout the process. In practice however, certain knowledge of the sediment properties may be obtained and thus make the problem less undetermined. For example, by incorporating knowledge of the sound speed ratio, the profiles in Figures 28 and 29 can be adjusted such that the sound speed profile intersects the seafloor at the measured sound speed of the sediment. Through conventional seismic methods, information on the deep layering structure may be established which will place lower bounds on the perturbation integral. Although not used in these analyses since only low grazing angle data were collected, the deep earth algorithm described in a subsequent section could have accurately identified the sedimentary layers

shown in Figure 18. By incorporating this type of information into the inversion, the solution is less undetermined and converges rapidly to a solution.

In order to test the accuracy of the shallow site inversion, model estimates of TL were compared with measured TL values. For the 50 Hz case, the results from BG1 were used as the input to FEPE. It is evident from Figure 28 that the derived sound speed profile suggests a two layer sedimentary sequence consisting of a lower speed sediment overlying a higher speed layer. The rather sharp transition in sound speed at about 35 m in depth indicates a rather abrupt change in lithology which we interpret as the change from the silty-clay layer to the sand. Therefore, generic values of sediment density and compressional attenuation were incorporated in the inverse geoacoustic model to account for this transition. For the 140 Hz case (Figure 29), the results from BG1 were modified in a similar fashion to incorporate the change in density and attenuation with depth.

Figures 30 and 31 show a comparison of the TL curves measured at the shallow site with the TL curves found through pertubative inversion technique for the same receiver combinations as in the previous section. Also shown in the figures are TL versus range results using the geoacoustic model derived in Section II. As evident from the curves, the perturbative inversion model results in estimates of TL that are as good or in some case better than using a high resolution geoacoustic model as input to the acoustic propagation models.

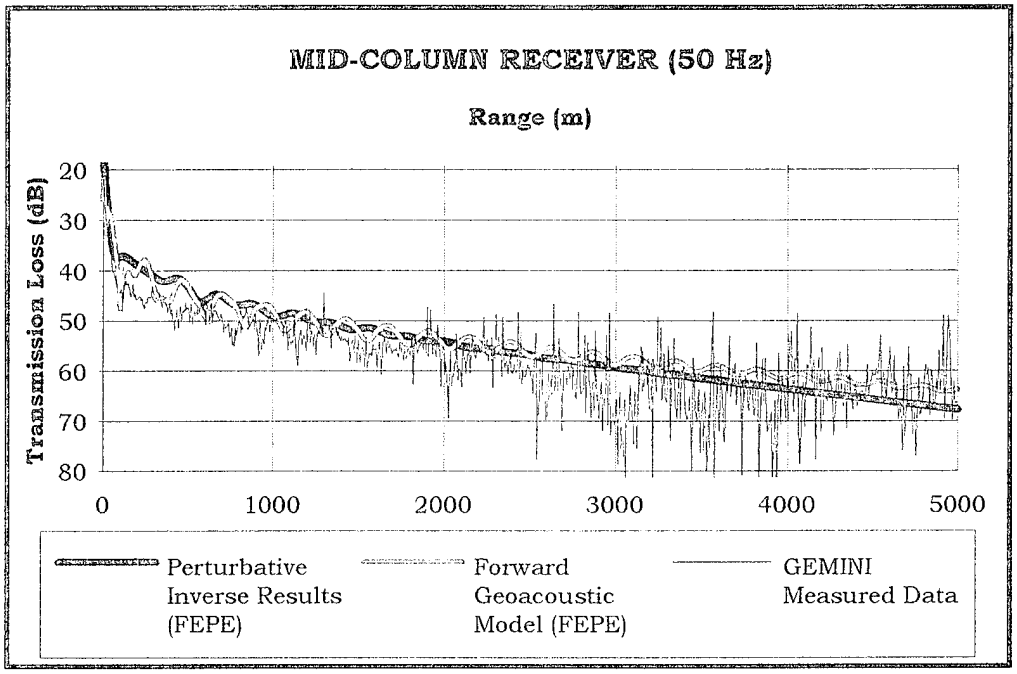

(a)

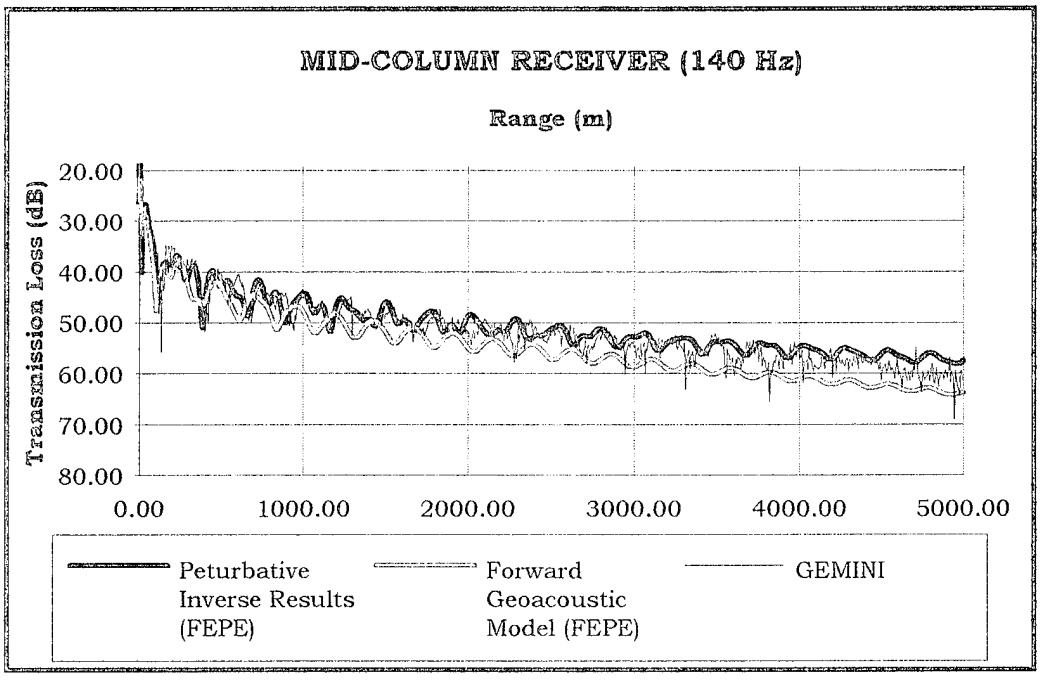

(b)

Figure 30. Plot of GEMINI TL data versus FEPE using as input the perturbative inverse solution and a site specific geoacoustic model for the mid-column receiver, shallow site. Frequency : 50 Hz (a), 140 Hz (b).

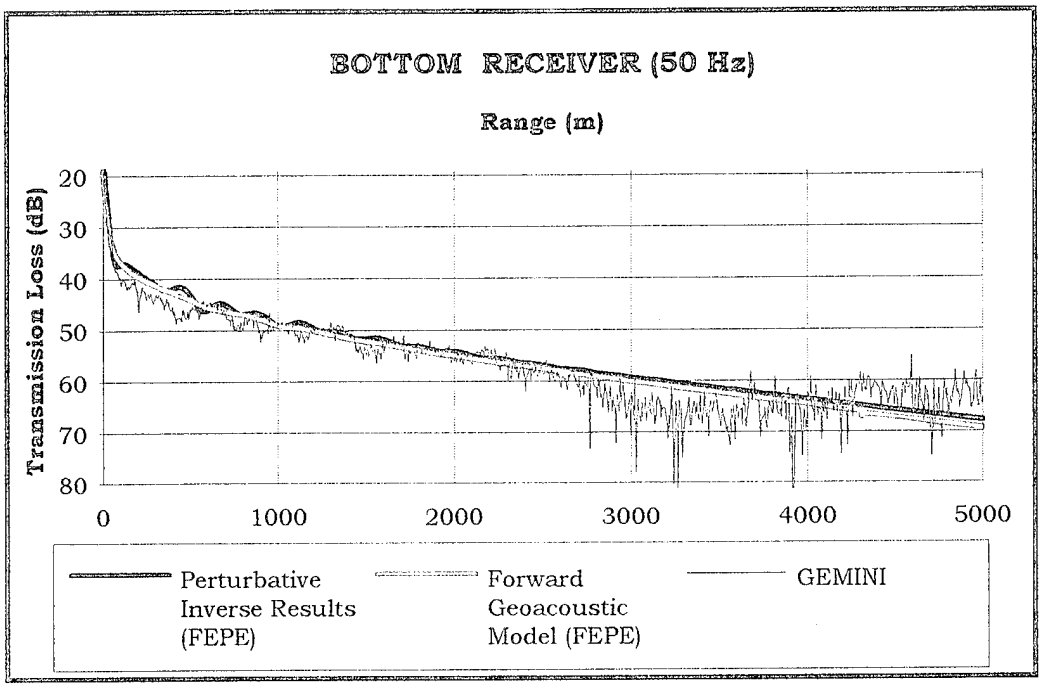

(a)

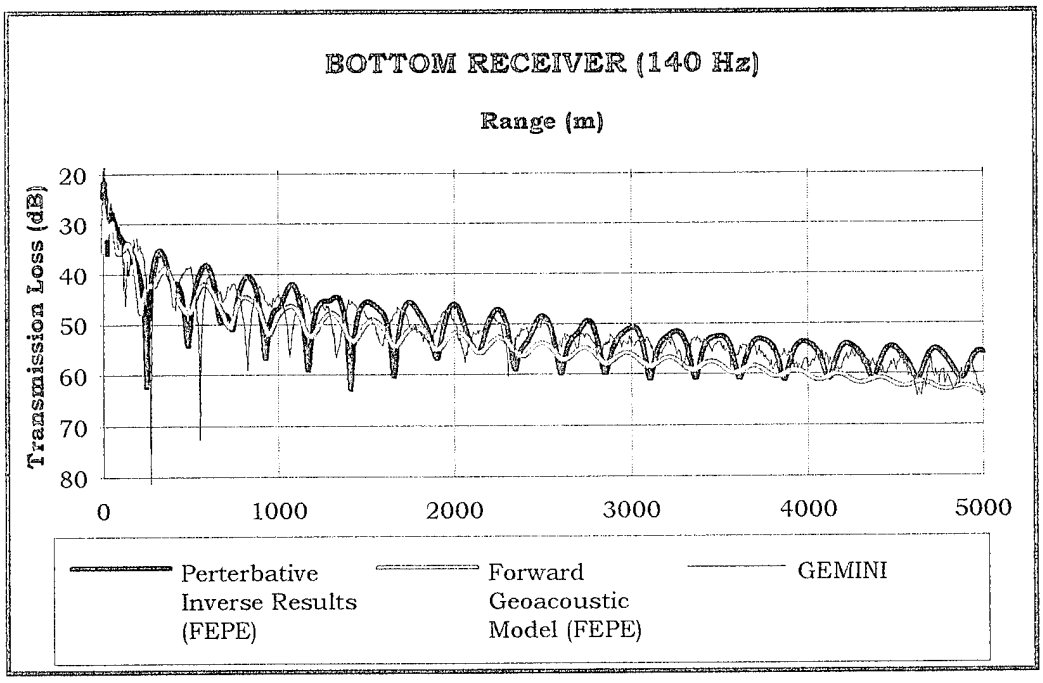

(b)

Figure 31. Plot of GEMINI TL data versus FEPE using as input the perturbative inverse solution and the site specific geoacoustic model for the bottom receiver, shallow site. Frequency : 50 Hz (a), 140 Hz (b).

B. DEEP SITE

The Green's function versus horizontal wavenumber plots for the deep site are shown in Figures 32 and 33. As with the shallow site, these plots are the result of Hankel transforming the experimental pressure field over the entire propagation path. Typically, as frequency and water depth increase, the number of trapped mode substantially increases. This is made apparent by the large number of poles of the Green's function. The eigenvalues for the two frequencies are tabulated in Table 10. The 50 Hz plot (Figure 32) shows two distinct peaks at horizontal wavenumbers of about 0.203 m^{-1} and 0.197 m^{-1}. A weak pole is also evident at about a horizontal wavenumber of about 0.190 m^{-1}. The 140 Hz plot shows four distinct modes situated at horizontal wavenumbers of about 0.57, 0.55, 0.54, and 0.52 m^{-1}. However, only the latter three, more energetic modes were actually used in the inversion, since the pole at the horizontal wavenumber of 0.57 did not correlate with results from the mid-column receiver.

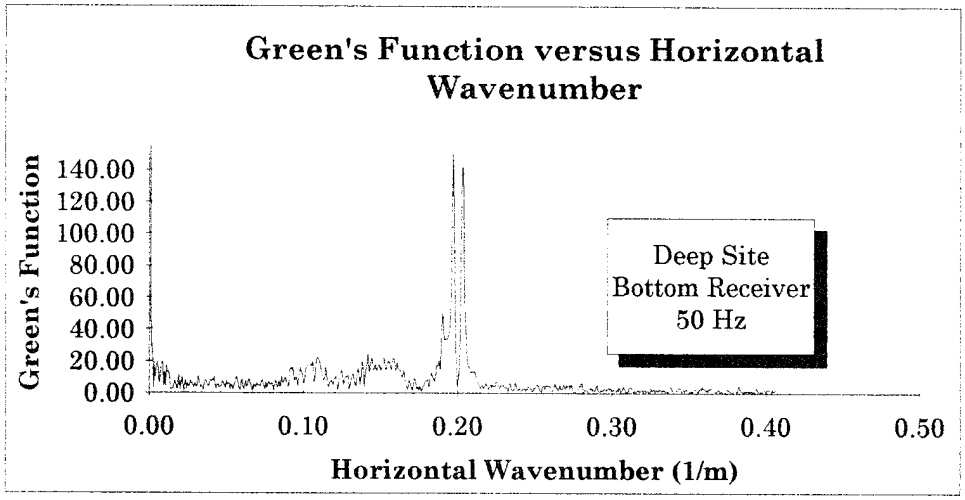

Figure 32. Magnitude of the depth dependent Green's function at 50 Hz for the deep site experiment. Only the bottom receiver is shown.

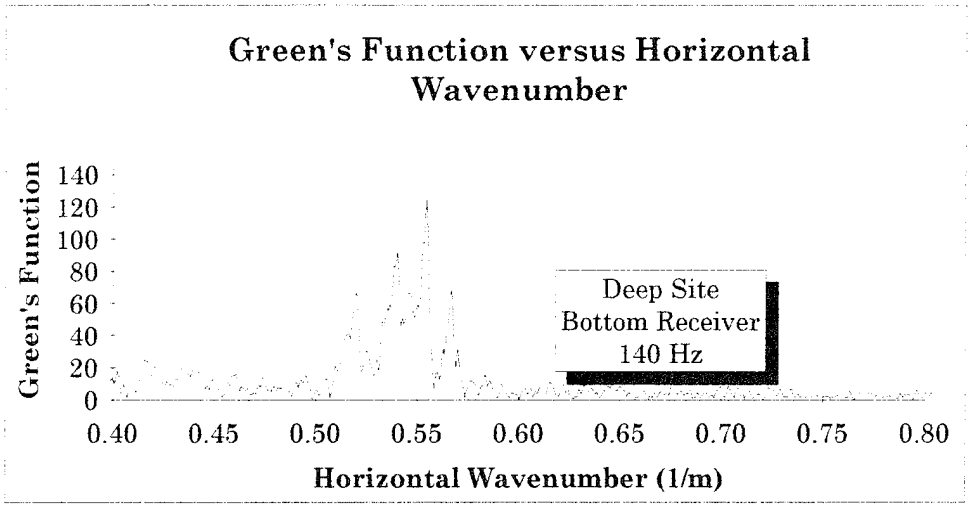

Figure 33. Magnitude of the depth dependent Green's function at 140 Hz for the deep site experiment. Only the bottom receiver is shown.

Frequency (Hz)	Mode Number	k_{meas} (m^{-1})
50	1	0.20322170900693
	2	0.19715011547344
	3	0.19012702078522
140	1	0.55415575176589
	2	0.54314384460141
	3	0.52018249243189

Table 10. Measured mode eigenvalues for the deep site.

Using the modes shown in Table 10, the perturbative inverse was performed separately for each frequency at the deep site. Unlike the shallow site, the inversion process at the deep site was extremely sensitive to the initial background model used. The initial background models BG1 and BG2 used in the previous section resulted in an unstable inverse solution. One explanation for this is that low order eigenvalues in the Backus-Gilbert decomposition result in an undetermined inverse matrix which causes the solution to become unstable. However, several experimental iterative runs showed that a background model starting with a reduced initial sound speed of c(0) = 1400 m/s, and a constant gradient of $\nabla c = 2.0\ s^{-1}$ coupled with a constant density of $\rho = 1.56\ g/cm^3$, provided a stable sound speed profile. The

results of the 50 Hz inversion are displayed in Figure 34 along with the site specific geoacoustic model developed previously.

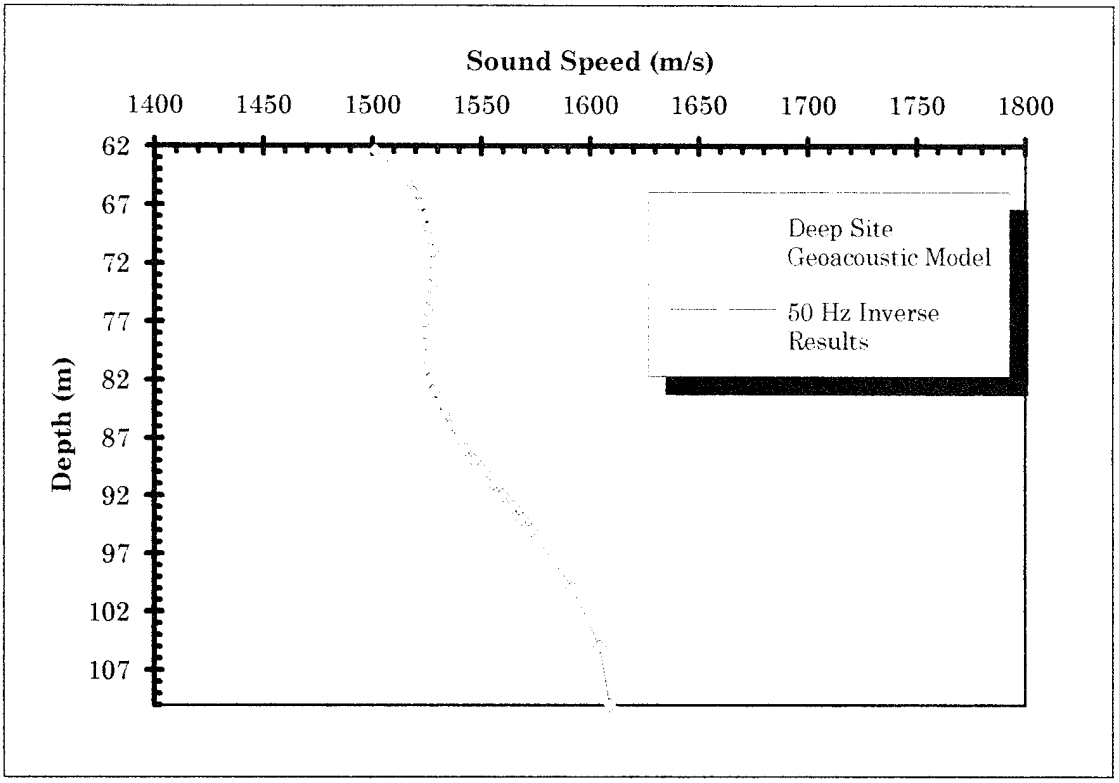

Figure 34. Results of the 50 Hz perturbative inversion at the deep site. The deep site geoacoustic model derived in Section III is also shown.

Using the same initial background geoacoustic model as for 50 Hz, the results of the 140 Hz perturbative inversion are shown in Figure 35. In order to stabilize the fluctuations in c(z), a "box-car" average was once again applied to the 140 Hz inverse solution. Both the 50 Hz and 140 Hz sound speed profiles suggest that the upper sedimentary layer at the deep site extends deeper than indicated in the geoacoustic model. This is a valid result, since as discussed previously, the thickness of the Holocene age silty-clay layer varies substantially in the GEMINI region.

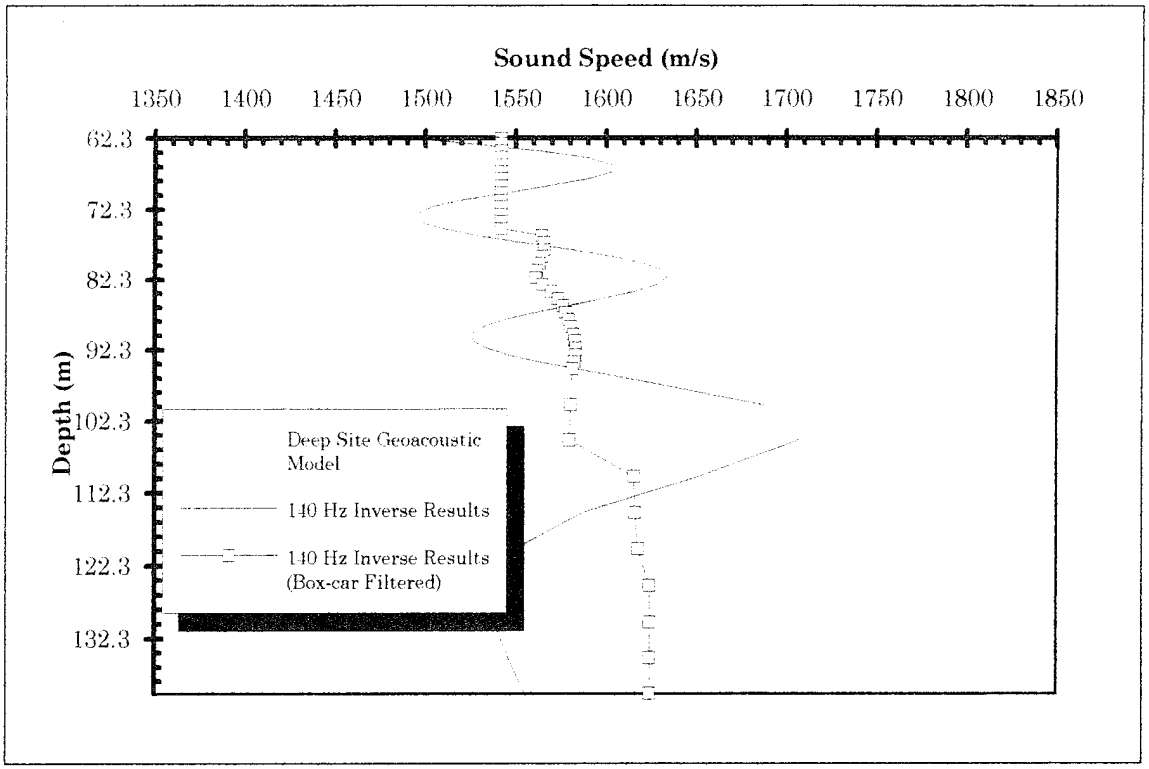

Figure 35. Results of the 140 Hz perturbative inversion at the deep site. The deep site geoacoustic model derived in Section III is also shown.

Using values consistent with Hamilton (1978, 1980), the above sound speed profiles were adjusted to account for varying sediment density and compressional attenuation with depth. The resulting geoacoustic models were used as input to FEPE. Figures 36 and 37 show a comparison of the TL curves measured at the deep site with FEPE estimates of TL using the results of the corrected inversion as input. As evident from the figures, the estimates of TL generated by the perturbative inverse solution are extremely consistent with the measured TL values.

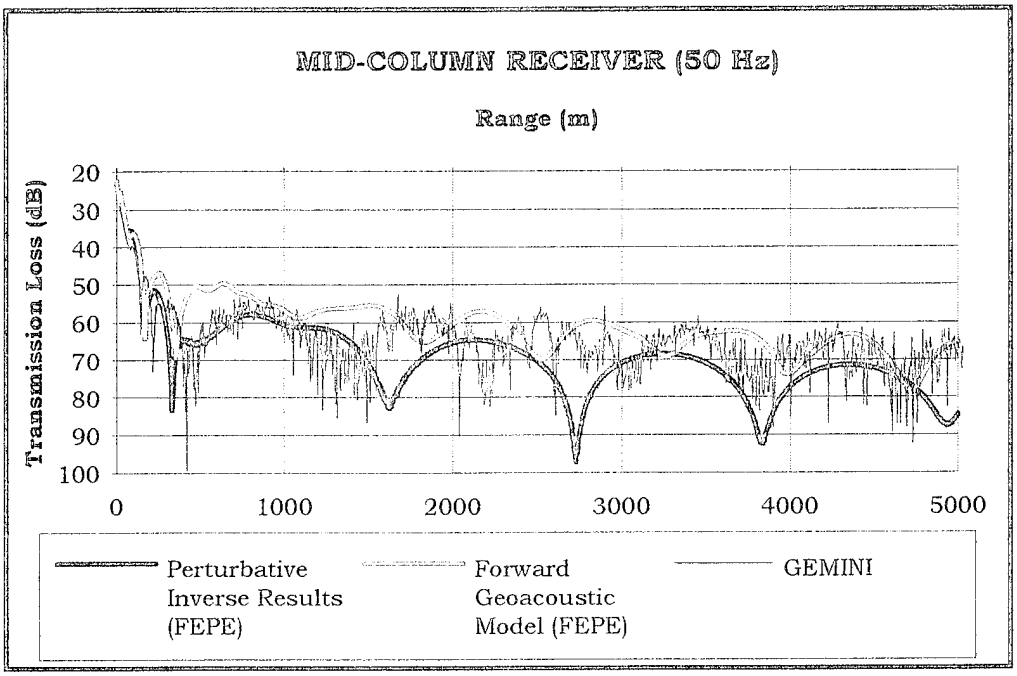

(a)

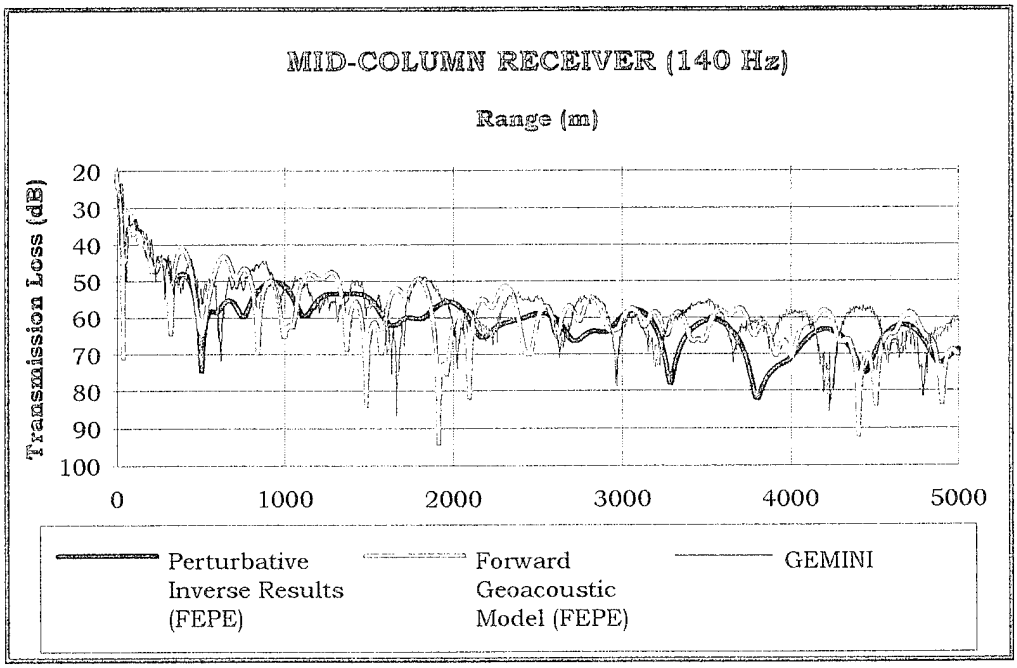

(b)

Figure 36. Comparison of GEMINI TL data and FEPE TL model estimates using as input the perturbative inverse solution and the site specific geoacoustic model for the deep site for a mid-column receiver. Frequency: 50 Hz (a), 140 Hz (b).

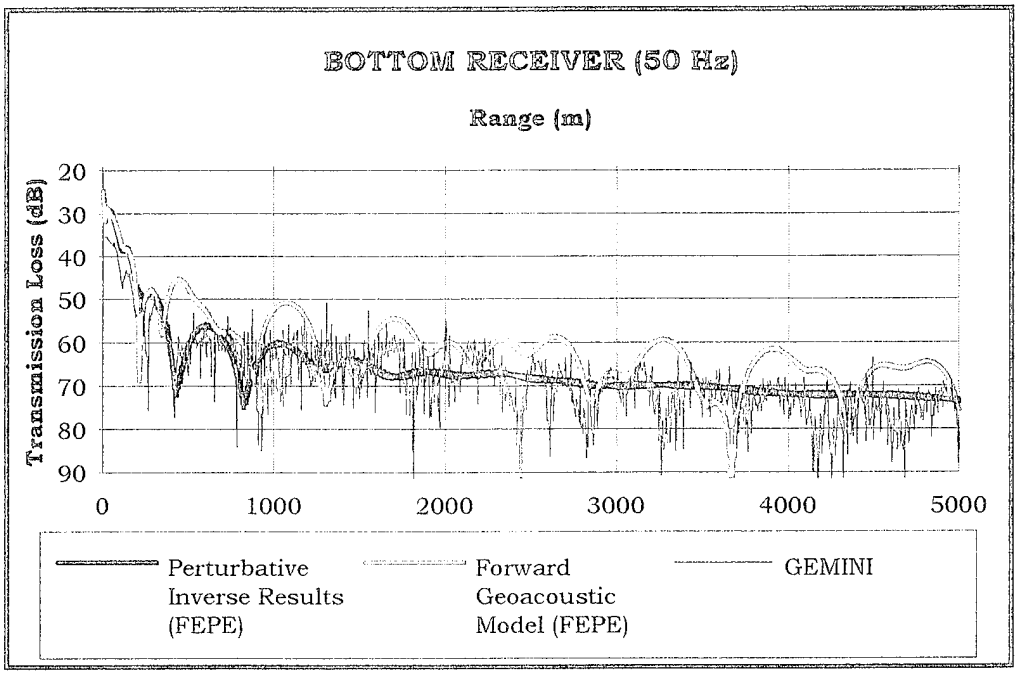

(a)

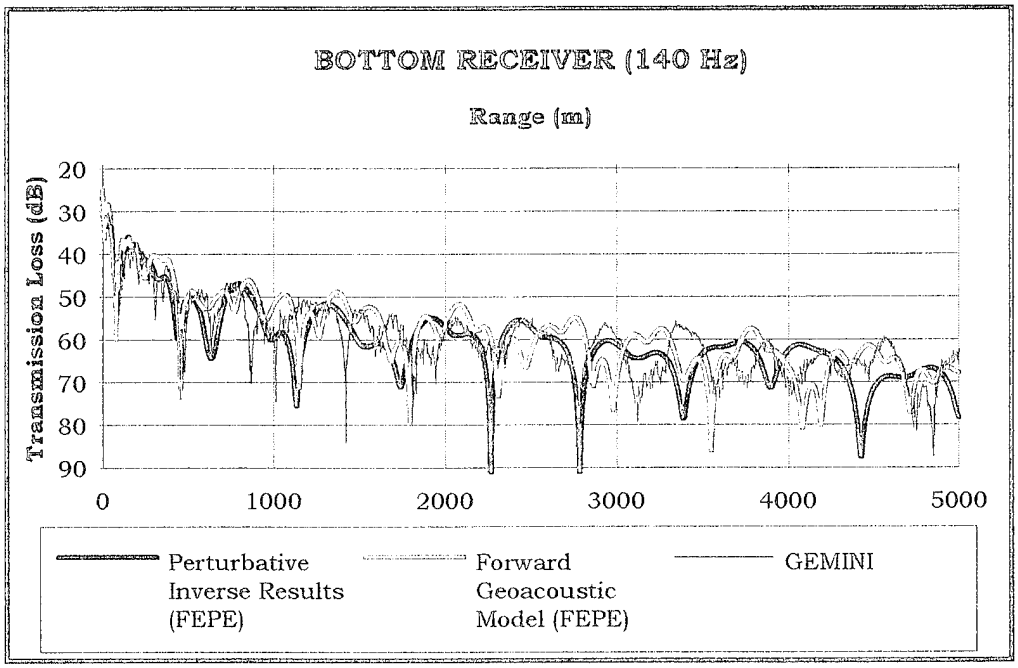

(b)

Figure 37. Comparison of GEMINI TL data and FEPE TL model estimates using as input the perturbative inverse solution and the site specific geoacoustic model for the deep site for a bottom receiver. Frequency: 50 Hz (a), 140 Hz (b).

C. DEEP EARTH SEISMIC MODEL

The inverse technique developed in this thesis relies principally on shallow grazing angle (< 20°) propagation in estimating the near surface geoacoustic parameters. Typically, using this inversion method, geoacoustic parameters can be accurately resolved to about 4/3 of an acoustic wavelength down from the seafloor. Inasmuch as low angle propagation paths are important for this inversion technique and more importantly in typical ASW scenarios, the technique is not effective in identifying underlying sediment layers beyond 4/3 acoustic wavelengths.

To augment the capability of the inverse technique, conventional seismic reflection methods are proposed to resolve these deeper sediment structures. These methods typically rely on higher propagation grazing angles (> 45 °) and thus are able to penetrate deeper into the seafloor. Therefore, a deep earth model is required to account for these deeper geologic horizons. A deep earth model was not applied to experimental data in this thesis; however a brief discussion is provided in this section to show how this information may be incorporated into the perturbative inverse technique.

The proposed deep earth model is developed from high angle (> 45 °) propagation paths and low (< 25 Hz) source frequencies. The supporting data can be collected simultaneously as the data collected for the inverse technique by collecting an adequate sample of short range (i.e., high angle) time-series. Subsequently, the processing then follows standard seismic signal processing procedures as follows:

Step 1: The time series data are stacked or gathered using common midpoint (CMP) stacking algorithms.

Step 2: The data set is deconvolved to remove artifacts from the data such as water borne reverberation.

Step 3: Normal move out (NMO) corrections are applied to the CMP stacks.

Step 4: Frequency filter the data with a time dependent, bandpass filter. The bandpass filters are constructed in a manner to allow lower frequencies to pass as two way travel time increases.

Step 5. In range-dependent sub-bottom environments, time and depth migration schemes should be employed to identify lateral discontinuities in the strata (i.e., faults, intrusions, etc.)

Step 6: Display data in a distance versus two-way travel time plot such that geologic lithologies and structures can be identified.

If steps 1 through 6 were applied to the GEMINI data, the sediment interface between the Holocene age silty-clay layer and the late Wisconsin age sand layer could be easily discerned by source frequencies as high as 50 Hz. Incorporating the exact position of the layer into the inversion would reduce the undetermined state of the inverse solution and ultimately would improve the final product. The Navy now has the low frequency capability (e.g., HLF-1 sonar on submarines) on board and thus the deep earth model is very practical and cost effective. The deep earth model should be considered part of the inverse technique algorithm recommended for use in the fleet.

V. CONCLUSIONS AND RECOMMENDATIONS

The technical approach in this thesis addressed two methods of estimating geoacoustic parameters for acoustic propagation modeling. In the first part of the study propagation model estimates of TL were compared with measured low-frequency acoustic propagation data collected during Project GEMINI. Location-specific, high resolution geoacoustic models of the sub-bottom were input to the acoustic models in the first part of the study. The geoacoustic models derived in this section were constructed in manner described in Hamilton (1980) and made use of available geologic and geophysical data The acoustic models examined in this portion of the study were the SACLANTCEN normal mode acoustic propagation model (SNAP), and the NRL finite element parabolic equation model (FEPE). The comparisons were made over two source frequencies (50 and 140 Hz) at two depth settings (mid-column and near-bottom setting). Overall, it was shown that FEPE, using as input the detailed site specific geoacoustic characterizations, resulted in estimates of TL that were more accurate than those calculated by SNAP and were reasonably consistent with the measured TL field. Moreover, it was shown that TL estimates are extremely sensitive to the input environmental parameters. Even in a seemingly range-independent acoustic environment such as off the Texas coast, a small change in a geoacoustic parameter (e.g., sediment thickness) can result in a significant change in TL.

In the second part of this study, the perturbative inversion technique (Rajan, 1987) was used to estimate the geoacoustic parameters for the two GEMINI sites. The objective of perturbative inversion is to estimate the depth variation in geoacoustic parameters in the sub-bottom (i.e., sound speed, density, attenuation, etc.) from the differences between the horizontal wave numbers from measured data and the corresponding wavenumbers computed for a background geoacoustic model. To illustrate the efficacy of

the inverse method, the initial background geoacoustic model used in the inversion assumed no *a priori* information of the seafloor. The resultant inverse solution was used to predict the geoacoustic properties at each of the sites. As a measure of effectiveness, estimates of TL using the inverse results (modeled with FEPE) were directly compared to the measured GEMINI TL values. The final results were in excellent agreement with the measured TL and the resulting TL estimates were as good as or better than the TL estimates obtained from detailed, site-specific geoacoustic models.

By assuming no *a priori* information in the inversion process and subsequently obtaining such excellent results in TL addresses an extremely critical problem for the U. S. Navy in shallow water regions. In many of the strategic, littoral environments knowledge of the geoacoustic properties of the sub-bottom is extremely limited. Direct geologic and geophysical surveys in these regions to determine relevant geoacoustic environmental parameters are both costly and time consuming and generally not consistent with the rapid response requirements of today's fleet. Therefore, the use of perturbative inversion technique is an accurate, cost effective and practical alternative to obtaining acoustic performance prediction estimates in these regions. Data necessary for the inversion can be easily collected using existing Navy platforms and hardware.

Automation of the inversion algorithm presented in this thesis could allow for an entire range of initial background models to be implemented in the inversion process. At present, one background model is assumed and after each iteration of the inversion, a set of eigenvalues and eigenfunctions are generated by the normal mode program (KRAKEN). However, in a fully automated mode, an entire range of background models with differing initial sound speeds and sound speed gradients could be analyzed by the inversion routine consecutively. By applying this method, a family of sound speed profiles can be formulated. This is especially applicable in high noise

environments where the eigenvalues of the inverse matrix are exceptionally small.

Currently, there are numerous existing pressure field data sets (e.g., Bearing Stake, NATIVE I, Southwest Florida Sea Test, etc.) that the inversion method, as described in this thesis, can be readily applied. To test the robustness of the inversion, several environmental scenarios should be examined ranging from a weakly range-dependent environment such as the Southwest Florida shelf to a more geologically complex region such as the Northern Arabian Sea (Bearing Stake exercise). Finally, it is recommended that an at-sea experiment be conducted using fleet assets to collect the required pressure field data.

LIST OF REFERENCES

Akal, T., "Sea floor effects on shallow-water acoustic propagation," in *Bottom Interacting Ocean Acoustics*, edited by W. A. Kuperman and F. B. Jensen, Plenum, New York (1980).

Backus, G., and F. Gilbert, "Uniqueness in the inversion of inaccurate gross earth data," *Philos. Trans. R. Soc. London*, 266, 123-192, (1970).

Berryhill, H. L. and A. R. Tippet, "Map showing post-wisconsin sedimentation patterns and faulting in the Corpus Christi 1 x 2 quadrangle, Texas," U. S. Geological Survey, Misc. Inv. Ser. Map I-1287-D, Denver, CO (1981).

Casey, K. D., "A modal/WKB inversion method for determining sound speed profiles in the ocean and ocean bottom," Engineer's thesis, MIT/WHOI Joint Program, Cambridge, MA and Woods Hole, MA, (June 1988).

Clay C. S. and H. W. Medwin, *Acoustical Oceanography*, John Wiley & Sons, New York, (1977).

Duarte, S. P., "A comparative study of acoustic models in a range-independent shallow water environment," Master's thesis, Naval Postgraduate School, Monterey, CA, December (1994).

Evans, K. E., "A normal mode model for estimating low-frequency acoustic transmission loss in the deep ocean," Ph.D. diss., Naval Postgraduate School, Monterey, CA, September (1975).

Fryer, G. R., "Reflectivity of the ocean bottom at low frequency," *J. Acoust. Soc. Am.* 63(1), 35-42 (1978).

Frisk, G. V., A. V. Oppenheim, and D. R. Martinez, "A technique for measuring the plane-wave reflection coefficient of the ocean bottom," *J. Acoust. Soc. Am.* 68(2), 602-612 (1980).

Frisk, G. V., J. F. Lynch, and J. A. Doutt, "The determination of geoacoustic models in shallow water," in *Ocean Seismo-Acoustics*, edited by T. Akal and J. M. Berkson, Plenum, New York (1986).

Frisk , G. V., J. F. Lynch, and S. D. Rajan, "Determination of compressional wave speed profiles using modal inverse techniques in a range-dependent environment in Nantucket Sound, "*J. Acoust. Soc. Am.* 86(5), 1928-1939 (1989).

Haberman, R., *"Elementary Applied Partial Differential Equations,"* 2nd Edition, Prentice Hall, Englewood Cliffs, NJ, (1987).

Hamilton, E. L., "Compressional-wave attenuation in marine sediments," *Geophysics.* 37, 620-646 (1972).

Hamilton, E. L., "Sound attenuation as a function of depth in the sea floor," *J. Acoust. Soc. Am.* 59(3), 528-535 (1976).

Hamilton, E. L., "Sound velocity-density relations in sea-floor sediments and rocks," *J. Acoust. Soc. Am.* 63(2), 366-377 (1978).

Hamilton, E. L., "Sound velocity gradients in marine sediments," *J. Acoust. Soc. Am.* 65, 909-922 (1979).

Hamilton, E. L., "Geoacoustic modeling of the seafloor," *J. Acoust. Soc. Am.* 68(5), 1313-1340 (1980).

Jensen, F. B., W. A. Kuperman, M. B. Porter, and H. Schmidt, *Computational Ocean Acoustics*, AIP, Woodbury, NY (1994).

Lynch, J. F., S. D. Rajan and G. V. Frisk, "Perturbative inversion methods for obtaining bottom geoacoustic parameters in shallow water," *in Progress in Underwater Acoustics*, edited by H. M. Merklinger, Plenum Press, New York, (1987).

Lynch, J. F., S. D. Rajan and G. V. Frisk, "A comparison of broadband and narrow-band inversions for bottom geoacoustic properties at a site near Corpus Christi, Texas," *J. Acoust. Soc. Am.* 89(2), 648-665 (1991).

Matthews, J. E., P. J. Bucca and W. H. Geddes, "Preliminary environmental assessment of the Project GEMINI site - Corpus Christi, Texas," Naval Ocean Research and Development Activity, Rep. No. 120 (1985).

Mitchell, S. K. and K. C. Focke, "New measurements of compressional wave attenuation in deep ocean sediments," *J. Acoust. Soc. Am.* 67(5), 1582-1589 (1980).

Morton, J. F., "The shallow water diesel: a new priority," *Naval Institute Proceedings*, 119(3), 126-128 (1993).

O'Keefe, S., F.B. Kelso, and C. E. Mundy, "From the sea-Preparing the naval service for the 21st century," Washington, D. C.: U. S. Government Printing Office, (1992).

Porter, M. B., "The KRAKEN Normal Mode Program," SACLANTCEN Memorandum Serial No. SM-245, (1991).

Rajan, S. D., J. F. Lynch and G. V. Frisk, "Perturbative inversion methods for obtaining bottom geoacoustic parameters in shallow water," *J. Acoust. Soc. Am.* 82, 998-1017 (1987).

Rajan, S. D. and G. V. Frisk, "Seasonal variations of the sediment compressional wave-speed profile in the Gulf of Mexico, "*J. Acoust. Soc. Am.* 91, 127-135 (1992).

Rajan, S. D., Personal communication with the author, Naval Postgraduate School, Monterey, CA, December (1994).

Ross, C., E. Kelly, L. Reynolds, M. Neil and J. Bowman, "A summary of sediment size, sound velocity and mass physical properties of 16 cores and 15 grab samples from the Gulf of Mexico," USNS LYNCH. U. S. Naval Oceanographic Office, Lab Item 508 (1978).

Rubano, L. A., "Acoustic propagation in shallow water over a low-velocity bottom," *J. Acoust. Soc. Am.* 67(5), 1608-1613 (1980).

Urick, R. J., *Sound Propagation in the Sea* (Defense Advanced Research Projects Agency, Washington, DC, 1979).

Zhou, J. X., X. Z. Zhang, P. H. Rogers., and J. Jarzynski, "Geoacoustic parameters in a stratified sea bottom from shallow water acoustic propagation," *J. Acoust. Soc. Am.* 82(6), 2068-2074 (1987).

Withers, J. D., "Anti-submarine warfare: considerations for future operations in third world regions," Naval War College, Newport, RI (November, 1992).

INITIAL DISTRIBUTION LIST

		No. Copies
1.	Defense Technical Information Center Cameron Station Alexandria, VA 22304-6145	2
2.	Library, Code 52 Naval Postgraduate School Monterey, CA 93943-5101	2
3.	Chairman (Code OC/BF) Department of Oceanography Naval Postgraduate School Monterey, CA 93943-5000	3
4.	Naval Meteorology and Oceanographic Command 1020 Balch Boulevard Stennis Space Center, MS 39529-5005 Attn: RADM P.G. Gaffney C. Wilcox	2
5.	Commanding Officer Naval Oceanographic Office Stennis Space Center, MS 39529-5001 Attn: Dr. Landry Bernard Dr. Martha Head Library	3
6.	Commanding Officer Naval Research Laboratory Code 5110/5123 Washington, DC 20375-5000 Attn: Dr. H. Fleming Mrs. S. Owen Dr. T. C. Yang Dr. R. Heitmeyer	4

7. Officer in Charge — 4
Naval Research Laboratory
Stennis Space Center, MS 39529-5004
Attn: Dr. P. Bucca
Dr. S. Chin-Bing
Dr. D. King
Mr. J. McDermid

8. Commanding Officer — 5
NCCOSC RDTE DIV
53560 Hull St.
San Diego, CA 92152-5001
Attn: Capt. K. E. Evans
Dr. J. Roese
Dr. H. Bucker
Dr. F. Ryan
Dr. R. Bachman

9. Dr. James H. Wilson — 5
Neptune Sciences, Inc.
3834 Vista Azul
San Clemente, CA 92674

10. Ms. Josie Fabre — 2
Neptune Sciences, Inc.
150 Cleveland Ave.
Slidell, LA 70458

11. Mr. Jim Donald — 1
Naval Undersea Warfare Center
New London Lab
Code 01Y
New London, CT 06320

12. Mr. Barry Blumenthal — 1
Code C124A
Advanced Environmental Acoustic Support Program
Office of Naval Research
800 N. Quincy St.
Arlington, VA 22217-5660

13. Dr. Bill Cary — 1
ARPA/MSTO
3701 N. Fairfax Drive
Arlington, VA 22203-1714

14. Dr. Subramaniam Rajan — 1
Woods Hole Oceanographic Institution
Applied Ocean Physics and Engineering Department
Woods Hole, MA 02543

15. Mr. Ed Chaika/Mr. Dave Small — 2
Advanced Environmental Acoustic Support Program
Code ONR - DET
Building 1020 - Room 184
Stennis Space Center, MS 39529-5000

16. Commanding Officer — 2
Space and Naval Warfare Systems Command
Dept. of the Navy
2451 Crystal Drive
Arlington, VA 20245-5200
Attn: Captain W. Hatcher
Dr. R. Cockerill

17. LT J. Mark Null — 2
14374 Old Pearsall Road
P. O. Box 206
Lytle, TX 78052

18. The University of Texas — 1
Walter Geology Library
Austin, TX 78713-9953